

Functional Polymers for Bone Tissue Engineering Applications

Jie Song

Materials Sciences Division, Lawrence Berkeley National Laboratory, University of California,

Berkeley, CA 94720, USA

Email: jsong@lbl.gov

Phone: 1-510-486-4125

Fax: 1-510-486-4995

and

Carolyn R. Bertozzi

Departments of Chemistry and Molecular and Cell Biology, and Howard Hughes Medical
Institute, University of California, Materials Sciences Division, Lawrence Berkeley National

Laboratory, Berkeley, CA 94720, USA

Email: bertozzi@cchem.berkeley.edu

Phone: 1-510-643-1682

Fax: 1-510-643-2628

Table of Contents:

1. Introduction
2. Functional synthetic hydrogel scaffolds for hard tissue engineering applications
 - 2.1 Environmentally responsive functional hydrogels mimicking collagenous ECM as growth factor carriers
 - 2.2 Functional hydrogels mimicking mineral-binding anionic noncollagenous ECM proteins
 - 2.3 High-affinity integration of functional hydrogels with biominerals
3. Functional self-assembling polymer scaffolds for template-driven biomineralization
 - 3.1 Amphiphilic self-assembling thin films
 - 3.2 Polymerizable self-assembling peptide-amphiphile nanofibers
 - 3.3 Bolaamphiphilic self-assembling polymer ribbons
 - 3.4 Extension of 2-D bolaamphiphilic self-assembling polymer templates to 3-D composites
4. Concluding remarks

1. Introduction

Bone serves many essential functions in the body. It protects organs, provides structural support, provides a scaffold for muscle attachment, generates blood cells and helps maintain essential ion levels. Therefore, the pathology of bone can be very serious. As the average age of the population increases, the demand for artificial materials to assist or replace organ functions and improve quality of life is rapidly increasing. The National Center for Health Statistics (NCHS) reports that 152,000 total hip replacements, 299,000 knee replacements and 59,000 revisions of hip and knee replacements were performed in 2000 alone.[1] The American Dental Association estimates that the number of root-form dental implants is likely to grow approximately 4% per year to ~610,000 implants in 2003.[2]

Synthetic materials currently used in the fabrication of orthopedic implants were originally developed for non-biological applications. They tend to consist of a single bioinert material, such as metals, ceramics or polymers, or of a relatively coarse combination of two or three components. Although these synthetic materials do provide an immediate solution for many patients, their long-term outcomes are not satisfactory.[3-5]

There are three major limitations of existing implant materials. First, these materials exhibit serious mechanical property mismatches with their surrounding native tissues and thus lead to implant failure and/or cause tissue damage.[6] Osteoblasts, the bone-producing cells, respond to external stimulation such as mechanical stress by generating new bone.[7,8] Implants stiffer than natural bone (e.g. metallic implant) bear a major proportion of the mechanical load, shielding the surrounding skeleton from its normal stress level. As a result, osteoblasts are discouraged from making new bone at the implant-tissue interface, which eventually leads to slow resorption of surrounding bone tissue and loosening of the implant. On the other hand,

ceramics such as calcium phosphates provide favorable osteophilic environment for bone cells,[9,10] but are rather weak in terms of mechanical resistance. Their application tends to be limited to low-stress locations, such as broken jaws or fractured skulls.[11-14]

Second, these materials typically do not bear functionalities that encourage communication with their cellular environment, therefore limiting the potential for tissue attachment and ingrowth.[15] In natural bone, there are bone cells (osteoblasts and the bone-resorbing osteoclasts) and a myriad of soluble factors and extracellular matrix components that are constantly involved with the bone formation and remodeling process.[16] Unlike natural bone, existing bone implants cannot self-repair or adapt to changing physiological conditions.[17]

Third, in the case of composite implants, there is a lack of control of structural features (on both microscopic and nanoscopic levels) and adhesion strength (both between various components of the composite and at the implant-tissue interface). In contrast, nature combines organic matrices with inorganic components with highly controlled hierarchical microstructures in the design of skeletal tissues.[8,18-21] With the exception of enamel, all structural calcified tissues including bone and dentin are biological composites of collagen, a protein-based hydrogel template, and inorganic dahilite (carbonated apatite) crystals of similar composition, but varying microstructures. Collagen provides a structural framework for the integration with calcium apatites and the attachment of acidic matrix proteins that regulate the biomineralization and remodeling processes. In addition, collagen endows bone with the necessary toughness to complement the strong yet brittle mineral component.[8] The unusual architectural combination of a hard inorganic material and an underlying elastic hydrogel network gives native bone unique mechanical properties, such as low stiffness, resistance to tensile and compressive forces and

high fracture toughness.[8,22] For instance, the Young's modulus for collagen fibers that form the organic matrix of bone, is typically 0.1-2 GPa.[23] The value for apatite, the inorganic component of bone, is around 110 GPa.[24] The Young's Modulus of cortical bone is between 10 and 20 GPa,[25] an intermediate value that reflects the unique integration of collagen and apatite. The interfacial adhesion of the organic and inorganic components also contributes to these properties.

The development of bonelike composites with improved mechanical properties and enhanced biocompatibility over traditional implants calls for a biomimetic synthetic approach using natural bone as a guide. The very complex nature of bone's structure and the poorly understood nature of bone biogenesis have hindered real biomimetic design of artificial bone. By using a bottom-up synthetic approach, however, one can start with simple model systems with well-defined chemical, physical and biological properties, and then gradually increase the complexity of the system to realize a higher order approximation of the natural bone. Indeed, impressive progress has been made in this direction, with some recent examples demonstrating that bone-like properties can be engendered in wholly synthetic systems.[26,27] Information gathered from the bottom-up synthetic approach should prove valuable for a better understanding of bone synthesis, including the process of template-driven biomineralization. The goal of this approach is to derive a set of rules to guide future rational design of functional composite materials with desired mechanical, chemical and biological properties.

In this chapter, we focus on recent progress in using functional polymers, particularly functional hydrogels and self-assembling polymers as templates for biomimetic artificial bone-like composites. Emphasis will be placed on the bottom-up design strategy, the introduction of

desired biological function and the control of organic-inorganic interfaces within the composite material.

2. Functional synthetic hydrogel scaffolds for hard tissue engineering applications

Limitations associated with traditional orthopedic implants have driven the exploration of alternative materials as bone tissue engineering scaffolds. Naturally derived bone-tissue engineering scaffolds include cornstarch-based polymers,[28] chitosan,[29] collagen,[30] and marine coral.[31] Synthetic inorganic bone mimics are primarily calcium phosphates.[32-34] Synthetic organic scaffolds used in bone-tissue engineering include mainly poly(α -hydroxy acids),[3,35,36] poly(phosphazenes),[37] poly(caprolactones),[38] and poly(propylene fumarates).[39] Composites of organic and inorganic materials have also been used as bone grafting scaffolds.[40-42]

Among all, marine coral exoskeletons that are capable of being hydrothermally converted to hydroxyapatite, and various biodegradable poly(α -hydroxy acids) including poly(glycolic acid) (PGA), poly(lactic acid) (PLA) and poly(lactic-*co*-glycolic acid) (PGLA), are the most widely used substrates, partly due to their FDA approved status for *in vivo* applications. However, intermediate acidic degradation products of these poly(α -hydroxy acids) can lead to undesired local pH change surrounding the implant and generate inflammatory responses.[43-46] In addition, the chemical degradation of the polymer scaffold could also lead to degradation of its mechanical properties ahead of the occurrence of desired tissue ingrowth. Last but not the least, poly(α -hydroxy acids) have limited functionalizability. It is particularly difficult to modify the polymers with multiple functional domains, which has increasingly been recognized as an essential element in the design of real biomimetic scaffolds. Therefore, there is a strong need for

alternative functional polymers that can overcome the limitations of poly(α -hydroxy acids), and allow for better approximation to the natural system.

Hydrogels are water-swollen, cross-linked structures produced by a covalent polymerization of one or multiple types of monomers. Additionally, hydrogels can form from non-covalent association of building blocks via an extensive hydrogen bonding network or strong van der Waals interactions. Hydrogels have unique physical properties such as elasticity and water retention ability that resemble those of natural hydrogels, and chemical versatility. Thus, functionalized hydrogels, in either degradable or non-degradable forms, have long been appealing candidates for the design of soft tissue engineering scaffolds.[47-49] However, their potential for hard tissue engineering applications has only been explored relatively recently. Here, we review some recent examples with an emphasis on 1) the design of crosslinked networks with environmentally responsive linkers to allow the emulation of collagen as growth factor carriers;[27] 2) the introduction of multiple functional domains including mineral nucleating ligands to mimic the templating and regulatory role of non-collagenous extracellular matrix component (ECM);[26,50] and 3) the integration of hydrogel scaffolds and osteophilic biomaterials with enhanced adhesion strength at the polymer-mineral interface.[51,52]

2.1 Environmentally responsive functional hydrogels mimicking collagenous ECM as growth factor carriers

The complexities of skeletal biology were recently reviewed in a series of articles in Nature.[53-56] Bone synthesis and remodeling is the interplay of mineral deposition and resorption by specialized bone cells, a process that is constantly occurring on a microscopic scale across our skeleton. During this process, a myriad of growth factors, distributed in either soluble or attached form throughout the cavities of bone, play critical roles.[16] For instance, bone

morphogenic protein-2 (BMP-2), a member of the transforming growth factor- β (TGF- β) superfamily that promotes ectopic bone formation, modulates the organization and expression of osteoblastic cell proteins. Specifically, it was shown that BMP treatment stimulated adhesion and proliferation of osteoblastic cells, and this adhesive advantage was reflected in enhanced long-term matrix mineralization in the BMP-2 pretreated cultures.[57,58] Recently, BMP was delivered using a biodegradable PLA-poly(ethylene glycol) (PEG) copolymer scaffold to induce ectopic bone formation in vivo.[59]

Collagenous ECM, in addition to providing structural and biochemical cues for cells in contact, is also susceptible to cell-triggered proteolysis,[60] which enables cell invasion and subsequent remodeling of the matrix, leading to bone regeneration. In a sense, collagen functions as a growth factor carrier for bone regeneration. The most commonly used existing synthetic growth factor carriers, such as PGA, PLA or PGLA,[61,62] however, were designed based on the passive mechanism of growth factor delivery, ignoring the complex interactions between cells and ECM in natural bone. Therefore, one necessary improvement in the design of biomimetic organic scaffolds for treating bone defects is to construct a 3-dimensional network where growth factors may be stored and bone cells may be allowed to invade in a controlled fashion. This requires the installation of a chemical trigger that responds to external stimuli.

Some synthetic matrices used in cell culture and tissue engineering have been developed to be responsive to physical[63,64] and biochemical stimuli.[65] Recently, a phosphate-containing crosslinked hydrogel composed of a linear poly/oligo(2-hydroxyethyl methacrylate) (HEMA) backbone, degradable ethyl phosphate linker groups and linear PEG macro-segments was prepared as a potential bone tissue engineering scaffold.[66] The degradation occurs at the site of the phosphate linker and results in the gel's gradual collapse into linear poly/oligoHEMA,

linear PEG, phosphoric acid and ethanol. The release of phosphoric acid could impact bone formation, although the concept has yet to be proved experimentally.

Synthetic scaffolds responsive to cellular stimuli, however, have not yet received the attention that they deserve. The most elegant example so far was recently reported by Hubbell and coworkers.[27] The team engineered synthetic PEG-based hydrogels containing pendant peptide ligands for cell adhesion and peptide-PEG linkers that are susceptible to degradation by matrix metalloproteases (MMPs). A schematic illustration of the assembling of the gel is shown in Figure 1. After incubating the gel with recombinant human bone morphogenic protein-2 (rhBMP-2), an osteoinductive growth factor, the composite was implanted to a site of defect in the rat crania. A month later, the implant was found to be invaded by host cells and remodeled into bony tissue.[27] The authors contribute the localized bone regeneration to the susceptibility of the gel to cell invasion and the entrapment of osteoinductive growth factors such as BMPs. This work elegantly illustrates that biological recognition principles adopted by natural ECM components may be engendered in a synthetic hydrogel scaffold via careful rational design.

2.2 Functional hydrogels mimicking mineral-binding anionic noncollagenous ECM proteins

Another fundamental challenge in mimicking the function of natural bone with synthetic scaffolds is to emulate nature's strategy for template-driven biomineralization. In natural bone synthesis, it has been suggested that the biomineralization process starts with the formation of transient amorphous calcium phosphates (although the direct detection of these transient precursors is difficult[67,68]) and poorly crystalline apatites.[68,69] These precursors then undergo several crystalline phase transitions, such as brushite, octacalcium phosphate and tricalcium phosphate, before the more stable crystalline HA finally forms.[19] Organic matrices

are postulated to be involved in both supramolecular pre-organization and interfacial molecular recognition, critically influencing the heterogeneous nucleation rate and the orientation of crystal growth. The process begins with the nucleation and formation of nanometer-sized particles, both of which are promoted by anionic protein ligands that are rich in aspartate, or glutamate and/or phosphoserine residues.[70,71] The epitaxial relationship between the crystal lattice spacing and the binding sites on the organic matrices can control the assembly of calcium phosphate nuclei.[72]

The exact role of individual acidic matrix proteins in mineralization is still far from understood. The nucleation activity of bone sialoprotein (BSP), a sialylated and phosphorylated protein expressed only in mineralized tissues and a potent nucleator of HA, appears to be linked to its glutamic acid rich sequences, which gives rise to a secondary structure of left-handed helix.[73] Its HA nucleating activity is not affected by dephosphorylation of the protein.[70] More recently, site-directed mutagenesis of the poly[E] regions in full-length rat BSP showed that replacing two domains of poly[E] with poly[D] does not alter the nucleating activity of the protein, suggesting the flexible nature of BSP may be advantageous to its function. However, the replacement of both poly[E] domains with poly[A] significantly decreased its HA nucleating activity, confirming the essential role of anionic residues.[74] The authors further demonstrated that a sequence of at least eight contiguous glutamic acid residues is required for the nucleation of HA by BSP and this minimal nucleating sequence does not constitute an α -helical conformation that was previously speculated as essential for HA binding.[74] The phosphoserine and aspartate-rich sequence in phosphophoryn, the main non-collagenous protein in dentin, on the other hand, has long been considered as essential in the mineralization of dentin.[71,75]

Because of the lack of a common understanding of how different anionic amino acid repeats contribute to the nucleation and crystal growth, a bottom-up approach that allows systematic introduction of different anionic ligands with increasing modular information and controlled spatial arrangements into a synthetic scaffold provides a valuable alternative to investigate the molecular details of template-driven biomineralization. The concept of recapitulating natural bone synthesis by using synthetic polymers functionalized to mimic the mineral nucleating acidic non-collagenous proteins is illustrated in Figure 2.

Our group has been particularly interested in applying functional hydrogels toward this end based on several attractive features of hydrogels. The intrinsic elasticity and water retention ability of synthetic hydrogels resemble those of natural hydrogels, such as collagen matrices that are prevalent as structural scaffolds in various connective tissues including bone.[47] The porosity of synthetic hydrogels may be controlled by various techniques including solvent casting / particulate leaching,[76,77] phase separation,[78] gas foaming,[79] solvent evaporation,[80] freeze drying,[81] blending with non-crosslinkable linear polymers,[82] and rapid prototyping[83,84] to afford a range of pore sizes to allow for pre-implantation cell seeding or post-implantation tissue ingrowth. More importantly, 3-dimensional hydrogel networks displaying multiple functional domains can be realized through copolymerization of several types of functional monomers (Fig. 3). The polymerization chemistry is water compatible, allowing incorporation of polar ligands such as anionic peptides that mimic the acidic matrix proteins regulating mineral growth, and biological epitopes such as the tripeptide RGD[85-89] that promote integrin-mediated cellular adhesion.

Specifically, we designed and synthesized a library of anionic methacrylamides to copolymerize with (2-hydroxyethyl methacrylate), or HEMA, to form 3-dimensional hydrogel

copolymers. As shown in Figure 3, these monomers vary in both the type (carboxylate or phosphate) and the number of ionic sites they carry. The phosphorylated tetrapeptide GDS*S* (where S* stands for phosphoserine) is derived from the known DS*S* repeat of bone phosphoproteins.[71,90,91] Tetrapeptide GDSS was designed as a non-phosphorylated control to probe the role of phosphorylation in template-driven mineralization in a synthetic model system. By varying the percentage of the anionic monomers incorporated, the average distance between potential nucleation sites can be controlled. Finally, GRGD, a tetrapeptide carrying the RGD motif that is known to contribute to the physical properties of bone extracellular matrix,[90] and critical for inducing cell adhesion and initiating the healing process,[86,87,89,92,93] was introduced to the hydrogel copolymer. All these monomers were synthesized via the direct coupling of the corresponding amino acids or oligopeptides with methacryloyl chloride in a buffered aqueous solution, in satisfactory to excellent yields.

The formation of hydrogel copolymers was realized using a standard radical polymerization protocol[48] with 2-10% of crosslinkers of various lengths. The freshly prepared gels were extensively washed in water before they were subject to mineralization or used for in vitro cell culture. We have shown that by varying the percentage of anionic monomers included, the porosity of the hydrogel copolymers can be tuned, with an average pore size up to hundreds of microns.

Cytotoxicity evaluation using the osteosarcoma cell line TE85 showed that these bone cells were able to adhere and proliferate on hydrogels containing up to 10% of anionic residues. When the adhesive motif GRGD was incorporated, cells were able to spread over the gels with morphologies very close to those attached to tissue culture polystyrene (TCPS) control.

We are now using microarray analysis to probe how attachment to these synthetic scaffolds affects the global gene expression profile of osteoblasts. One would like to ensure that cells are not activating an apoptotic (programmed cell death) pathway when they are exposed to the non-native bone substitute, and genes encoding important osteogenic proteins are regulated in a way that benefits the synthesis and secretion of ECM proteins and biominerals. One difficulty associated with interpreting the interactions of cells with 3-dimensional materials, however, is that it is hard to separate out the influence of surface chemistry from various other physical factors of the 3-D scaffold such as surface roughness, porosity and pore size of the gel. Therefore, we developed 2-dimensional model surfaces functionalized with the same library of anionic ligands and subjected them to in vitro cell culture. Our preliminary results show that bone cells grow and proliferate very well on these anionic surfaces, in many cases better than on TCPS. This suggests a favorable interaction between osteoblasts and mineral binding anionic motifs. A complete gene expression profile readout, when available, can guide us to intelligently modify the surface chemistry in the iterative design of next-generation of artificial bone-like materials.

Finally, it is worth noting that the incorporation of an appropriate percentage of anionic sites in the 3-dimensional hydrogel network may also contribute to the toughening of hydrogel-mineral composites. In addition to the mineral nucleating function, the anionic sites attached to the collagen matrix in natural bone have been suggested to be part of the energy-dissipating mechanism for bone. Recent AFM pulling and indentation studies of collagens and bone provide experimental evidence for the role of polymers as bridges between inorganic crystallites.[94] Unlike the apatite crystals that cannot dissipate much energy, “sacrificial” bonds, such as divalent cation-based ionic bridges between two anionic sites on the collagen scaffold,

have been suggested to deter crack propagation, and therefore improve the toughness of bone. This energy-absorbing toughening mechanism could be interesting to emulate in the rational design of new hydrogel-mineral composite materials.

2.3 High-affinity integration of functional hydrogels with biominerals

Without integration with biominerals such as calcium phosphates, synthetic polymer scaffolds alone do not provide the desired osteophilic environment and mechanical strength for load-bearing applications. There has been considerable effort to mimic bone by the mineralization of polymer substrates with hydroxyapatite (HA), the major inorganic component of natural bone. This is usually attempted through the time-consuming incubation of substrates with acellular simulated body fluid (SBF) with ion concentrations similar to those of human blood plasma.[95-98] Unfortunately, the process leads to slow growth of crystalline or amorphous biominerals that exhibit poor adhesion and lack a structural relationship with the substrate. Alternatively, composites could be formed by mixing HA powder with corresponding polymer solution (e.g. PGLA), followed by a thermally induced phase separation procedure.[99] The composite foams show improved mechanical properties over pure polymer foams. However, such simple mixing procedures typically do not confer the critical interfacial strength between the polymer phase and the mineral phase.

Efforts aimed at improving the interfacial adhesion strength between HA and polymers include the use of silane coupling agents,[100,101] zirconyl salts,[102] polyacids[103,104] and isocyanates.[105,106] Recently, chemical treatment of biodegradable PGLA films with aqueous base has been shown to facilitate the growth of crystalline carbonate apatite on the surface.[107] Both the morphology and thickness of the resulting crystalline apatite layer, however, suggest that it will suffer from inadequate interfacial adhesion (between the mineral and the polymer

substrate) and poor mechanical properties. Overall, composite materials that integrate organic scaffolds and HA, and demonstrate the level of integration of natural bone, have not yet been achieved.

pHEMA is one of the most widely used synthetic hydrogels in tissue engineering. Because of its high biocompatibility, pHEMA and its functionalized derivatives have been used as ophthalmic devices (e.g. contact lens),^[108,109] cartilage replacements,^[110] neural tissue engineering scaffold,^[111] bonding agents in dental resins and bone cements,^[112-114] and various drug delivery vehicles.^[115,116] However, its application as a 3-dimensional scaffold of artificial bonelike materials, has not been realized due to the lack of an effective approach to integrate it with inorganic minerals.

Therefore, we became interested in developing methods for the high affinity integration of pHEMA-based hydrogel scaffold and calcium apatites, specifically HA, a critical step towards the design and fabrication of pHEMA-based biomimetic bonelike composite materials. HA has limited solubility in water at neutral and basic pH.^[117] Based on this property, we designed a urea-mediated solution precipitation process where a segment of pHEMA hydrogel was thermally treated in an acidic solution (pH 2.5-3) of HA containing 2M urea.^[51] Upon gradual heating from room temperature to 95 °C, urea started to decompose and the pH slowly increased, promoting the hydrolysis of 2-hydroxyethyl side chains of pHEMA and allowing heterogeneous nucleation of calcium phosphate from sites of exposed carboxylates. A robust calcium phosphate layer up to several microns thick was obtained on the surface of the hydrogel, along with a high degree of calcification inside the hydrogel. The high affinity between the calcium ions and the in situ generated carboxylates translates into a low interfacial energy between the hydrogel and the

calcium phosphate, and consequently a low energy barrier for the heterogeneous nucleation of mineral onto the hydrogel scaffold. This sequence of events is depicted in Scheme 1.

Scanning electron microscopy (SEM) analysis revealed that the strong affinity between calcium ion and the surface carboxylates led to the 2-dimensional outward growth of calcium phosphate from individual nucleation sites (Fig. 4A) until the circular mineral layers merged and covered the entire surface (Fig. 4B). The strong adhesion between the apatite layer and the gel surface was evidenced by microindentation analysis performed on the surface of the composite (Fig. 4C). No delamination of the mineral layer was observed by SEM after Vickers indentations with loads up to 15N. To the best of our knowledge, such a level of adhesion at the mineral-substrate interface has never been observed before with minerals formed on polymer scaffolds or collagen films using the traditional SBF mineralization approach.[95-98] It is the direct and extensive mineral-hydrogel contact established during this process that led to the 2-dimensional outward growth of robust mineral layers, contrasting the SBF-induced 3-dimensional growth of crystalline apatites that are loosely bound to the polymer substrates. In the latter case, mineral nucleation and growth are largely controlled by substrate-induced subtle local pH changes and /or local ion saturation instead of strong interactions between the two phases. The calibrated energy dispersion X-ray spectroscopy (EDS) area analysis (Fig. 4D) revealed a Ca/P ratio similar to that of synthetic HA. X-ray diffraction (XRD) analysis (Fig. 4E), however, indicated that the mineral layer grown here was either amorphous or nanocrystalline in nature. The order and alignment of the *in situ* generated surface carboxylates may be limited, and may not match with the crystal lattice of HA to allow epitaxial growth of large crystallites detectable by XRD.

The role of amorphous calcium phosphate in natural bone has not been as extensively studied as that of amorphous calcium carbonate (ACC) in other calcified organisms. In Ascidian

P. pachydermatina, stabilized ACC was suggested to not only serve as a temporary storage site for calcium and carbonate,[118-120] but also play a structural role. The combination of isotropic and generally less brittle amorphous components (ACC) with their harder and less soluble crystalline counterparts (calcite) is thought to be nature's strategy to modulate mechanical properties of such composites.[121] The generation of a robust nanocrystalline or amorphous calcium phosphate layer that strongly adheres to the hydrogel scaffold presents an additional handle for controlling the mechanical property of bone-like composite materials. Ultimately, it is the combination of all subcomponents, the organic matrix, and the amorphous and crystalline mineral phases that renders the observed mechanical properties in natural hard composite tissues.

We also investigated the influence of external factors such as stirring, heating rate and duration of mineralization on the pattern of mineral nucleation and growth.[52] Constant stirring, which promotes homogeneous precipitation of HA and inhibits the desired heterogeneous nucleation and growth of HA onto the hydrogel scaffold, had to be avoided. Furthermore, heating rate was found to influence both the number of initial nucleation sites generated and the extent of final mineral coverage at the hydrogel surface. Finally, by extending the mineralization process, mineral coatings with thickness up to several microns can be obtained.[52]

This urea-mediated mineralization strategy can be extended to other calcium phosphates and pHEMA based functional hydrogel copolymers. The in vivo resorption rates of calcium phosphates vary greatly. For instance, crystalline hydroxyapatite (HA) is hardly soluble and its resorption could take years while tricalcium phosphate is more soluble and its resorption typically occurs in months.[14] The mineralization method we developed can be applied to a range of calcium phosphates (CPs) to produce hydrogel-CP composites with tunable in vivo bio-resorbability. Further, as shown in Figure 5, when the method was applied to pHEMA-based

copolymers containing various mineral-binding anionic residues described in section 2.2, similar mineral growth patterns were observed, again with strong gel-mineral interfacial adhesion.[50] The resulting composites will be subjected to more extensive in vitro and in vivo evaluations. We are interested to learn how the underlying anionic mineral binding motifs direct the new mineral deposition by osteoblasts once the amorphous or nanocrystalline calcium phosphate layer of the composites is resorbed by osteoclasts.

Finally, as discussed in the previous section, we have shown that pHEMA based functional hydrogel scaffolds with average pore sizes up to hundreds of microns can be obtained simply by adjusting the percentage of anionic residues incorporated. Such porosity would be important for nutrient diffusion, cell penetration, tissue ingrowth and potential vascularization of the scaffold.[122] However, composite materials based on porous scaffolds tend to be mechanically weak. It still remains to be seen whether this newly developed mineralization method can improve mineral integration with porous hydrogel scaffolds, a challenging problem we and many others strive to solve.

3. Functional self-assembling polymer scaffolds for template-driven biomineralization

Many essential biological activities of bone, including metabolism, regeneration and resorption, are influenced by changes of bone structure on the nanoscopic level. For instance, matrix-mediated nucleation is believed to occur by an epitaxial mechanism, in which a lattice match between the acidic organic ECM and the nascent crystal lowers the interfacial free-energy barrier to critical nucleus formation.[123,124] It has been speculated that the regularly spaced acidic groups serve as binding sites for calcium ions and align them in an orientation that matches the apatite crystal lattice.[125] The recapitulation of this template-driven

biomineralization paradigm in a synthetic environment with structural control on a nanoscopic level requires the use of highly ordered molecular templates. Self-assembling polymers are attractive candidates for this application.

Self-assembling amphiphiles and bolaamphiphiles typically contain a hydrophobic lipid core and hydrophilic headgroup on either one end (amphiphile) or both ends (bolaamphiphile) of the molecule. At air-water interfaces or in aqueous solution, these molecules spontaneously form ordered aggregates such as thin films,[126-128] vesicles,[129] nanofibers[26] and nanoribbons,[130] driven by van der Waals interactions at the core and an extensive hydrogen bonding network at the polar ends. If polymerization sites of associating molecules are properly aligned, they can be polymerized into robust polymeric templates with a highly ordered display of surface functional groups, such as mineral binding motifs. These ordered binding motifs could potentially serve as templates for bone-like nanocomposites.[26,126]

3.1 Amphiphilic self-assembling thin films

Self-assembled monolayers (SAMs) serve as powerful model systems to study the epitaxial growth of organic and inorganic particles at an organic-inorganic interface.[131-133] Several elegant examples illustrating the control of calcite crystal nucleation by polymeric or unpolymerized SAMs on various solid supports have been reported.[126,134-136]

Charych and coworkers demonstrated that cooperative interactions that are commonly observed at the organic-inorganic interface in biological calcified tissues can also drive the co-alignment of calcite at the surface of Langmuir-Schaefer films of poly(10,12-pentacosadiynoic acid) (Fig. 6).[126] The self-assembling polydiacetylene film was shown to nucleate calcite at the (012) face, a plane parallel to the polymer membrane plane. The crystals were co-aligned with respect to the polymer's ene-yne conjugated backbone. The authors attribute the co-

alignment of the crystals and the specific nucleation face type to symmetry reduction in the polymer template, in addition to proper stereochemical match at the organic-inorganic interface. Structural re-orientation of the polymer matrix upon calcite mineralization was also observed via a chromatic transition in the polydiacetylene film, presumably as a consequence of the stereochemical fit optimization.

Aizenberg et al. reported oriented nucleation of calcite controlled by SAMs of alkanethiols terminated with various surface residues supported on Au and Ag films.[135,136] It was shown that anionic surfaces are generally more active in inducing nucleation of calcite, whereas SAMs terminated with cationic residues or aliphatic tails inhibit nucleation. Moreover, the authors demonstrated that different surface modifications led to the nucleation of calcite from different crystallographic planes, suggesting that the orientation of crystal growth may be fine-tuned by varying the surface chemistry of the underlying SAMs.

More recently, amphiphilic self-assembling thin films were also used to template the synthesis of carbonated apatites.[128] Groves and coworkers utilized a stearic acid monolayer at an air-water interface as template to synthesize a free-standing continuous amorphous precursor film of carbonated calcium phosphate, which was then sintered into a dense crystalline film.

These elegant experiments provide valuable insights into the factors that dictate template-driven biomineralization in simplified model systems. Conclusions drawn from these studies provide useful guidelines for the design of artificial bone-like composites. However, direct applications of these amphiphilic self-assembling thin-films in bone tissue engineering are restricted to the fabrication of thin inorganic crystalline films or surface modification of metal or alloy implants. In addition, most work chose to illustrate the principle of template-driven mineralization via the relatively well defined calcite model system. Overall, alternative self-

assembling polymer scaffolds that can be biomimetically integrated with calcium apatites, the more relevant mineral compositions of bone, and are scalable to bulk composites, are still highly desired.

3.2 Polymerizable self-assembling peptide-amphiphile nanofibers

The design and fabrication of a scalable bone-like synthetic matrix based on the principle of self-assembly and biomimicry is an ambitious undertaking. Stupp and coworkers recently met the challenge by a clever design of sophisticated supramolecular aggregates of peptide-amphiphiles (PAs) bearing multiple functional domains to realize template-driven nucleation and growth of crystalline hydroxyapatite.[26] This work sets an optimistic precedent for the bottom-up rational design strategy. Key structural features of the self-assembling PA, as illustrated in Figure 7, include 1) a long aliphatic (C16) lipid tail that is responsible for the self-assembly of the amphiphiles;[137] 2) four consecutive cysteine residues that function as potential crosslinkers of the self-assembly; 3) a phosphoserine residue as potential binding site for calcium ions and mediator of the mineralization of HA;[71] 4) an RGD motif exposed at the polar end of the molecule that promotes integrin-mediated cell adhesion,[85,89] and 5) a flexible linker between the self-assembling/polymerization domain (lipid anchor and cysteine repeats) and the mineralization/cell adhesion domain.

When this highly engineered peptide-amphiphile was assembled in water above a critical concentration, formation of a gel composed of nanofibers with uniform dimensions was observed. The concentration-dependent gelation property allowed for direct injection of the material into a site of bone defect to promote synthetic matrix-assisted bone tissue repair. It also opened the possibility of controlling the macroscopic shape and size of the synthetic scaffold by simply carrying out the gelation in a cast of desired 3-dimensional geometry. In addition, the

formation of a gel composed of well dispersed functional nanofibers exposed biomimetic functional domains throughout the 3-dimensional scaffold, allowing potential nucleation and growth of biominerals and cell-material interactions to occur across the entire synthetic matrix. These are all desirable features in the design of scalable bulk bone-like materials.

Once self-assembled, the PAs were crosslinked via the formation of disulfide bonds at the hydrophobic-hydrophilic interface of the amphiphilic nanofiber to enhance its structural integrity. More importantly, the Northwestern team demonstrated that after crosslinking, the fibers were indeed able to carry out their primary intended function, which is templating the mineralization of HA. Within 10 min of exposure to a mineralization solution composed of CaCl_2 and Na_2HPO_4 , the nucleation of minerals on the surface of nanofibers was visualized by transmission electron microscopy (TEM). By 30 min, the formation of mature plate-shaped polycrystalline HA throughout the surface of nanofibers was observed by TEM and confirmed by energy dispersion X-ray spectroscopy (EDS) and electron diffraction analyses. Importantly, the presence and orientation of the diffraction arcs corresponding to the 002 and 004 planes (with enhanced intensity with respect to the 211 plane) suggested preferential alignment of the crystals with their *c* axes along the long axis of the nanofiber, reminiscent of the alignment of collagen fibrils and HA crystals in natural bone.

The fast nucleation and growth of well-aligned nanocrystalline HA was attributed to the phosphorylated serine residue designed into the scaffold. In a control experiment, the replacement of phosphoserine with a serine residue abolished the ability of the fiber to template the growth of crystalline HA within the same mineralization time frame. The result underscores the importance of phosphorylation in inducing crystalline mineral growth, echoing suggestions based on the sequence analysis and conformational modeling of some non-collagenous ECM

proteins in calcified tissue.[71] However, it is important to note that no systematic investigation of the role of phosphorylation in template-driven mineralization has been conducted in a synthetic model. With some literature showing that HA nucleating activity is unaffected by dephosphorylation of bone sialoprotein,[70] it is important not to generalize the result shown here. Overall, this work showcases that it is possible to rationally design a self-assembling polymeric system with biomimetic functionality relevant to bone biogenesis.

3.3 Bolaamphiphilic self-assembling polymer ribbons

We are interested in designing functional self-assembling polymers that adopt defined microstructures in solution in order to systematically probe how sequence, structure and packing arrangement of anionic mineral binding residues influence nucleation and alignment during templated crystal growth. In addition, we are pursuing methods for incorporating these synthetic mineralization domains into a 3-dimensional environment, mimicking the dispersion of acidic non-collagenous ECM proteins throughout the collagen matrix in bone.

Our work on the mineralization of functional hydrogel scaffolds suggests that the spacing, order and alignment of the mineral nucleating domains displayed on the hydrogel scaffold are limited. They do not match with the crystal lattice of HA to allow epitaxial growth of large crystallites detectable by XRD.[51] In fact, technically it is difficult to distinguish whether the robust mineral layer adhered to the anionic surface residues via the urea-mediated mineralization[52] is amorphous or nanocrystalline in nature. Therefore, to achieve better structural control of the biomineralization template, especially on a sub-nanoscale level, we are interested in self-assembling polymers, specifically bolaamphiphilic polydiacetylenes (BPDAs), as templates with ordered surface display of various mineral nucleating groups.

When properly designed, bolaamphiphilic diacetylene lipids can self-assemble into various supramolecular structures such as nanoribbons in aqueous media, and be polymerized into robust BPDAs under UV irradiation.[130] It is known that the specific arrangement of amphiphilic molecules in aqueous solutions depends on a variety of competing interactions, such as van der Waals force (mainly among hydrocarbon tails), ionic and dipolar interactions, hydrogen bonding (headgroup region), and interactions with water molecules. Here, the design of bolaamphiphiles instead of amphiphiles was intended for enhancing the order of lipid packing arrangement via the strengthening of H-bonding interactions on both sides of the polar surfaces of the lipid aggregates. In nature, membrane-spanning bolaamphiphilic lipids provide extraordinary stability to archaeobacteria, a class of microorganisms that can resist extreme environmental conditions such as low pH, high temperature, and high salt.[138]

A library of bolaamphiphilic diacetylene lipids has been designed and synthesized (Fig. 8). The diacetylene unit is placed at the center of the hydrophobic core to maximize alignment of neighboring diacetylene units in different packing arrangements. As shown in Figure 8, bolaamphiphilic lipids **1-9** carry various polar groups (either neutral, anionic or zwitterionic) on one end of the molecule. The design is intended to probe how different polar residues can template the nucleation and growth of biominerals such as HA, when arranged in a well-defined 3-dimensional fashion. As discussed at length in section 2.2, the tetrapeptide GDS*S* (S* = phosphoserine) in lipid **8** was derived from a typical DS*S* repeat of bone phosphoproteins.^{71,90,91} By varying the percentage composition of **8** in a polydiacetylene assembly, the average spatial distance between the anionic peptide repeats can be controlled to approximate the natural system. The unphosphorylated version (lipid **7**) was designed to examine the role of phosphorylation in template-driven biomineralization. Lipids **3** and **4** were designed

for the same purpose. Because of the intriguing *in vivo* roles of glutamic acid, hydroxyamino acid (such as serine) and aspartic acid residues in stabilizing amorphous mineral precursors and templating crystalline mineral growth, respectively,[121] we also designed lipid **5**, **6** and **3** to directly address this issue in a synthetic setting. Bolaamphiphile **1** carries a neutral amino ethylene glycol end group and is designed to dope the highly charged assembly to alleviate possible unfavorable electrostatic interaction at the assembly surface. Doping anionic PDA assemblies with less sterically hindered and less electron-rich lipids was useful for fine-tuning the assembly's polymerization behavior as well as the morphology of the aggregates.[139]

All lipids shown in Figure 8 were synthesized by coupling the N-terminus of corresponding free or protected amino acid or peptide to a common precursor, the N-hydroxysuccinimide (NHS) activated lipid **10**. [130,140] Self-assembly of most bolaamphiphilic lipids occurred rapidly upon probe sonication and low temperature incubation.[130] UV-irradiation in most cases instantaneously led to photopolymerization of the well-aligned diacetylene groups to form extended ene-yne conjugation backbone, resulting in formation of colored polymers.[140]

Extensive structural characterization was performed on selected bolaamphiphilic polydiacetylenes. As shown in Figure 9, TEM analysis and contact mode atomic force microscopy (AFM) analysis of BPDA formed by bolaamphiphile **5** showed that the polymer adopts either flat sheet (Fig. 9, panel A) or twisted ribbon (Fig. 9, panel B) morphologies, with highly ordered hexagonal and pseudo-rectangular surface packing arrangements, respectively. These ribbons are typically micron scale in length and nanometer scale in width and thickness. The ordered matrix of surface anionic residues generated here provides an excellent template for

probing which specific surface residues or sequences affect epitaxial nucleation and growth of crystalline HA or the stabilization of amorphous calcium phosphates.

We have shown that a number of anionic BPDAs template the growth of crystalline calcium apatites in less than 30 min upon the exposure to mineralization solution composed of CaCl_2 and Na_2HPO_4 . By contrast, BPDA terminated with neutral surface residues does not. Correlations between packing arrangement of underlying BPDA templates, conformations of surface residues and the observed oriented crystal growth, however, are yet to be established, but are a subject of future interest.

3.4 Extension of 2-D bolaamphiphilic self-assembling polymer templates to 3-D composites

When ordered BPDA mineral-binding domains are combined with porous, elastic, and highly functionalizable 3-D hydrogels, synthetic scaffolds with richer modular information may be derived. These scaffolds would better resemble the chemical and structural environment, physical properties, as well as biological functions of the highly integrated ECM of natural bone. To realize this potential, we designed a diacetylene bolaamphiphile with terminal methacrylamide functionality for covalently attaching BPDA templates to methacrylamide-based hydrogels. By varying the percentage of this linker molecule dispersed with other bolaamphiphiles, the distribution density of the mineralization domains within the hydrogel network can be modulated.

We are also pursuing an alternative polyelectrolyte strategy for stacking ordered BPDA mineralization templates into a 3-D composite with improved mechanical properties. In the early 1990s, Stupp and coworkers prepared a number of organoapatites via the co-precipitation of biominerals and polyelectrolytes (e.g. poly-*L*-lysine, poly-*L*-glutamic acid, poly-sodium acrylate).[141-144] They found that simultaneously mixing two oppositely charged

polyelectrolytes (e.g. poly-*L*-lysine and poly-*L*-glutamic acid) with calcium phosphate could result in composites that are more stable and mechanically more robust than those obtained by mixing one polyelectrolyte component with the biomineral.[143] Taking this strategy a step further, we propose to use a layer-by-layer deposition strategy, illustrated in Figure 10, to create BPDA-HA composite with mineral layers sandwiched in-between oppositely charged ordered BDPA templates.

4. Concluding remarks

Polymers with defined chemical functionality, shape and structural features are among the most promising and versatile building blocks for biomimetic bone-like materials. Engineered via rational design, hydrogels with multiple specialized functions may be quickly assembled via water compatible polymerizations to encode diverse features including integrin-mediated cell adhesion, environmental and cellular responsive degradations, and intelligent surfaces promoting mineral nucleation and crystal growth. Self-assembling polymers serve as excellent template for nanostructured composite materials. Their potential in bone tissue engineering is enormous, especially if the polymers can be properly integrated with a 3-dimensional scaffold.

This review focuses on organic matrix directed synthesis of composite scaffolds. It is worth noting that there is an alternative, which is to start with a porous inorganic scaffold and then infiltrate it with suitable polymers. Rapid prototyping (or solid freeform fabrication) processes may be used in the preparation of 3-dimensional inorganic scaffolds with fairly sophisticated architectural features.[84] For instance, direct ceramic stereolithography was achieved using UV-curable suspensions of HA powders in acrylates in a conventional stereolithography apparatus (SLA) machine.[145-147] A target HA structure was first designed

using computer assisted design (CAD) software or computer tomography (CT) data. The negative image of the design was then used to build an epoxy mold on the SLA. A thermal curable suspension of HA powder in acrylate was then cast into the epoxy mold and cured. Finally the epoxy mold and the acrylate binder were ablated, and the HA was fully sintered.[145] The common laser spot size used in SLA to solidify acrylics and epoxy resins is around 250 μm in diameter, resulting from a compromise between the precision demand and the maximum speed. Using recently developed small-spot SLA, components can be built up in steps that are less than 1 μm thick with a resolution finer than 10 μm . The maximum product size is currently limited to 35 mm^3 . [84]

Viscosity control for the highly concentrated suspension and cure depth behavior are the main challenges for fabricating 3-D porous ceramic patterns using stereolithography techniques.[148] In addition, broader applications of this process in tissue engineering also depend on the successful development of new photopolymerizable, biocompatible, and biodegradable liquid polymer materials.

Finally, the direct involvement of cells, although not the focus of this review, is essential for successful tissue regeneration upon the implantation of a synthetic scaffold. To ensure a maximal participation of cells, tissue engineering scaffolds can be made by either seeding cells into preformed interconnected porous water-insoluble matrices,[149] or injecting hydrogel materials that would gel within the body in response to a triggering mechanism, such as a temperature change or light irradiation.[150,151] Recently, a strategy was reported for assembling porous scaffolds loaded with cells in situ.[152] In situ gelling strategies has the advantage of being able to fill a cavity without knowing the precise dimension of the cavity and

the possibility of avoiding an invasive surgery for implantation. It may not be suitable, however, for load-bearing applications.

The bottom-up synthetic approach we showcase here uniquely complements, but could not replace, the traditional top-down approach adopted by bone biologists who focus on deciphering the secrets of bone synthesis based on native samples. To bridge the gap between synthetic bone-like materials and natural bone, the gap between the bottom-up and top-down approaches must be closed, starting with the integration of the most updated bone biology into the design of functional interfaces. In the case of bone-like composites, both the organic-inorganic interface and the tissue-material interface must be intelligently designed. This continues to be the major challenge of the field.

Acknowledgements:

This work was supported by the Laboratory Directed Research and Development Program of Lawrence Berkeley National Laboratory and the National Institute of Health grant No. R01 DE015633-01 under the Department of Energy Contract No. DE-AC03-76SF00098.

References:

- ¹ M. J. Hall and M. F. Owings, *2000 National Hospital Discharge Survey*, Vol. 329 (National Center for Health Statistics, Hyattsville, Maryland, 2002).
- ² American Dental Association, *Future of Dentistry* (American Dental Association, Health Policy Resources Center, Chicago, 2001).
- ³ W. Bonfield, in *European White book on Fundamental Research in Materials Science*, edited by M. Rühle, H. Dosch, E. J. Mittemeijer, and M. H. V. d. Voorde (Max Planck Institute für Metallforschung, Stuttgart, 2001).
- ⁴ F. S. Kaplan, W. C. Hayes, T. M. Keaven, A. L. Boskey, T. A. Einhorn, and J. P. Iannutti, (American Academy of Orthopaedic Surgeons, Columbus, OH, 1994), p. 127.
- ⁵ T. J. Webster, R. W. Siegel, and R. Bizios, *Nanostructured Materials* **12**, 983-986 (1999).
- ⁶ J. Black, *Biological performance of materials: fundamentals of biocompatibility*, 3rd, rev. and expanded ed. (Marcel Dekker, New York, 1999).
- ⁷ M. V. Hillsley and J. A. Frangos, *Biotechnol. Bioeng.* **43**, 573-581 (1994).
- ⁸ S. Weiner and H. D. Wagner, *Annu. Rev. Mater. Sci.* **28**, 271-298 (1998).
- ⁹ U. Ripamonti, *Biomaterials* **17**, 31-35 (1996).
- ¹⁰ H. Ohgushi, M. Okumura, S. Tamai, E. C. Shors, and A. I. Caplan, *J. Biomed. Mater. Res.* **24**, 1563-1570 (1990).
- ¹¹ C. J. Damien and J. R. Parsons, *J. Appl. Biomater.* **2**, 187-208 (1991).
- ¹² J. O. Hollinger, J. Brekke, E. Gruskin, and D. Lee, *Clin. Orthop. Relat. Res.*, 55-65 (1996).
- ¹³ R. A. Ayers, S. J. Simske, C. R. Nunes, and L. M. Wolford, *J. Oral Maxillofac. Surg.* **56**, 1297-1301 (1998).

- 14 C. Delloye, N. Cnockaert, and O. Cornu, *Acta Orthop. Belg.* **69**, 1-8 (2003).
- 15 G. Willmann, *Adv. Eng. Mater.* **1**, 95-105 (1999).
- 16 V. I. Sikavitsas, J. S. Temenoff, and A. G. Mikos, *Biomaterials* **22**, 2581-2593 (2001).
- 17 H. R. Piehler, *MRS Bull.* **25**, 67-70 (2000).
- 18 S. I. Stupp and P. V. Braun, *Science* **277**, 1242-1248 (1997).
- 19 S. Mann, *Biomineralization : principles and concepts in bioinorganic materials chemistry* (Oxford University Press, Oxford ; New York, 2001).
- 20 P. Ball, *Made to measure : new materials for the 21st century* (Princeton University Press, Princeton, N.J., 1997).
- 21 J. F. V. Vincent, *Structural biomaterials*, Rev. ed. (Princeton University Press, Princeton, N.J., 1990).
- 22 R. Baron, in *Handbook of experimental pharmacology; Vol. 107*, edited by A. B. Abou-Samra, G. R. Mundy, and T. J. Martin (Springer, Berlin ; New York, 1993), p. 111-147.
- 23 M. Balooch, I. C. WuMagidi, A. Balazs, A. S. Lundkvist, S. J. Marshall, G. W. Marshall, W. J. Siekhaus, and J. H. Kinney, *J. Biomed. Mater. Res.* **40**, 539-544 (1998).
- 24 W. Suchanek and M. Yoshimura, *J. Mater. Res.* **13**, 94-117 (1998).
- 25 J. J. Broz, S. J. Simske, W. D. Corley, and A. R. Greenberg, *J. Mater. Sci. - Mater. Med.* **8**, 395-401 (1997).
- 26 J. D. Hartgerink, E. Beniash, and S. I. Stupp, *Science* **294**, 1684-1688 (2001).
- 27 M. P. Lutolf, F. E. Weber, H. G. Schmoekel, J. C. Schense, T. Kohler, R. Muller, and J. A. Hubbell, *Nat. Biotechnol.* **21**, 513-518 (2003).
- 28 M. E. Gomes, A. S. Ribeiro, P. B. Malafaya, R. L. Reis, and A. M. Cunha, *Biomaterials* **22**, 883-889 (2001).

- 29 S. V. Madihally and H. W. T. Matthew, *Biomaterials* **20**, 1133-1142 (1999).
- 30 L. B. Rocha, G. Goissis, and M. A. Rossi, *Biomaterials* **23**, 449-456 (2002).
- 31 H. Petite, V. Viateau, W. Bensaid, A. Meunier, C. de Pollak, M. Bourguignon, K.
Oudina, L. Sedel, and G. Guillemin, *Nat. Biotechnol.* **18**, 959-963 (2000).
- 32 T. J. Flatley, K. L. Lynch, and M. Benson, *Clin. Orthop. Relat. Res.*, 246-252 (1983).
- 33 J. Goshima, V. M. Goldberg, and A. I. Caplan, *Clin. Orthop. Relat. Res.*, 274-283 (1991).
- 34 E. Kon, A. Muraglia, A. Corsi, P. Bianco, M. Marcacci, I. Martin, A. Boyde, I.
Ruspantini, P. Chistolini, M. Rocca, R. Giardino, R. Cancedda, and R. Quarto, *J. Biomed.
Mater. Res.* **49**, 328-337 (2000).
- 35 S. L. Ishaug-Riley, G. M. Crane-Kruger, M. J. Yaszemski, and A. G. Mikos, *Biomaterials*
19, 1405-1412 (1998).
- 36 C. M. Agrawal, D. Huang, J. P. Schmitz, and K. A. Athanasiou, *Tissue Eng.* **3**, 345-352
(1997).
- 37 C. T. Laurencin, S. F. ElAmin, S. E. Ibim, D. A. Willoughby, M. Attawia, H. R. Allcock,
and A. A. Ambrosio, *J. Biomed. Mater. Res.* **30**, 133-138 (1996).
- 38 C. E. Schmidt and J. B. Leach, *Annu. Rev. Biomed. Eng.* **5**, 293-347 (2003).
- 39 J. P. Fisher, T. A. Holland, D. Dean, P. S. Engel, and A. G. Mikos, *J. Biomater. Sci.,
Polym. Ed.* **12**, 673-687 (2001).
- 40 R. C. Thomson, M. J. Yaszemski, J. M. Powers, and A. G. Mikos, *Biomaterials* **19**, 1935-
1943 (1998).
- 41 K. G. Marra, J. W. Szem, P. N. Kumta, P. A. DiMilla, and L. E. Weiss, *J. Biomed. Mater.
Res.* **47**, 324-335 (1999).

- 42 P. X. Ma, R. Y. Zhang, G. Z. Xiao, and R. Franceschi, *J. Biomed. Mater. Res.* **54**, 284-
293 (2001).
- 43 B. L. Seal, T. C. Otero, and A. Panitch, *Mater. Sci. Eng., R* **34**, 147-230 (2001).
- 44 D. J. Trantolo, K.-U. Lewandrowski, J. D. Gresser, K. J. Bozic, and D. L. Wise, in
Biomaterials and Bioengineering Handbook, edited by D. L. Wise (Marcel Dekker, Inc,
New York, 2000), p. 603-618.
- 45 O. Bostman and H. Pihlajamaki, *Biomaterials* **21**, 2615-2621 (2000).
- 46 Y. H. An, S. K. Woolf, and R. J. Friedman, *Biomaterials* **21**, 2635-2652 (2000).
- 47 N. A. Peppas, *Hydrogels in Medicine and Pharmacy* (CRC Press, Boca Raton, 1986).
- 48 K. Y. Lee and D. J. Mooney, *Chem. Rev.* **101**, 1869-1879 (2001).
- 49 J. L. Drury and D. J. Mooney, *Biomaterials* **24**, 4337-4351 (2003).
- 50 J. Song, V. Malathong, and C. R. Bertozzi, (in preparation).
- 51 J. Song, E. Saiz, and C. R. Bertozzi, *J. Am. Chem. Soc.* **125**, 1236-1243 (2003).
- 52 J. Song, E. Saiz, and C. R. Bertozzi, *J. Eur. Ceram. Soc.* **23**, 2905-2919 (2003).
- 53 G. Karsenty, *Nature* **423**, 316-318 (2003).
- 54 W. J. Boyle, W. S. Simonet, and D. L. Lacey, *Nature* **423**, 337-342 (2003).
- 55 E. Zelzer and B. R. Olsen, *Nature* **423**, 343-348 (2003).
- 56 S. Harada and G. A. Rodan, *Nature* **423**, 349-355 (2003).
- 57 J. M. Wozney and V. Rosen, *Clin. Orthop.* **346**, 26-37 (1998).
- 58 A. K. Shah, J. Lazatin, R. Sinha, T. Lennox, N. J. Hickok, and R. S. Tuan, *Biol. Cell* **91**,
131-142 (1999).
- 59 N. Saito, T. Okada, H. Horiuchi, N. Murakami, J. Takahashi, M. Nawata, H. Ota, K.
Nozaki, and K. Takaoka, *Nat. Biotechnol.* **19**, 332 - 335 (2001).

- 60 Z. Werb, *Cell* **91**, 439-442 (1997).
- 61 A. J. Putnam and D. J. Mooney, *Nature Med.* **2**, 824-826 (1996).
- 62 L. D. Shea, E. Simley, J. Bonadio, and D. J. Mooney, *Nat. Biotechnol.* **17**, 551-554
(1999).
- 63 G. Chen and A. S. Hoffman, *Nature* **373**, 49-52 (1995).
- 64 W. A. Petka, J. L. Harden, K. P. McGrath, D. Wirtz, and D. A. Tirrell, *Science* **281**, 389-
92 (1998).
- 65 T. Miyata, N. Asami, and T. Uragami, *Nature* **399**, 766-9 (1999).
- 66 D.-A. Wang, C. G. Williams, Q. Li, B. Sharma, and J. H. Elisseeff, *Biomaterials* **24**,
3969-3980 (2003).
- 67 J. E. Roberts, M. Heughebaert, J. C. Heughebaert, L. C. Bonar, M. J. Glimcher, and R. G.
Griffin, *Calcif. Tissue Int.* **49**, 378-382 (1991).
- 68 J. E. Roberts, L. C. Bonar, R. G. Griffin, and M. J. Glimcher, *Calcif. Tissue Int.* **50**, 42-48
(1992).
- 69 H.-M. Kim, C. Rey, and M. J. Glimcher, *Calcif. Tissue Int.* **59**, 58-63 (1996).
- 70 G. K. Hunter and H. A. Goldberg, *Biochem. J.* **302**, 175-179 (1994).
- 71 A. George, L. Bannon, B. Sabsay, J. W. Dillon, J. Malone, A. Veis, N. A. Jenkins, D. J.
Gillbert, and N. G. Copeland, *J. Biol. Chem.* **271**, 32869-32873 (1996).
- 72 A. L. Boskey, *Ann. N.Y. Acad. Sci.* **760**, 249-256 (1995).
- 73 H. A. Goldberg, K. J. Warner, M. J. Stillman, and G. K. Hunter, *Connect Tissue Res.* **35**,
439-446 (1996).
- 74 C. E. Tye, K. R. Rattray, K. J. Warner, J. A. R. Gordon, J. Sodek, G. K. Hunter, and H.
A. Goldberg, *J. Biol. Chem.* **278**, 7949-7955 (2003).

- 75 A. Veis and A. Perry, *Biochemistry* **6**, 2409-2416 (1967).
- 76 C. E. Holy, M. S. Shoichet, and J. E. Davies, *J. Biomed. Mater. Res.* **51**, 376-382 (2000).
- 77 D. J. Mooney, L. Cima, R. Langer, L. Johnson, L. K. Hansen, D. E. Ingber, and J. P. Vacanti, *Mater. Res. Soc. Symp. Proc.* **252**, 345-352 (1992).
- 78 J. J. Klawitter and S. F. Hulbert, *J. Biomed. Mater. Res. Symp.* **2**, 161-229 (1971).
- 79 L. D. Harris, B.-S. Kim, and D. J. Mooney, *J. Biomed. Mater. Res.* **42**, 396-402 (1998).
- 80 A. G. Mikos, G. Sarakinos, S. M. Leite, J. P. Vacanti, and R. Langer, *Biomaterials* **14**, 323-330 (1993).
- 81 K. Whang and K. E. Healy, in *Methods of Tissue Engineering*, edited by A. Atala and R. P. Lanza (Academic Press, San Diego, San Francisco, New York, Boston, London, Sydney, Tokyo, 2002), p. 697-704.
- 82 J. H. Brauker, V. E. Carr-Brendel, L. A. Martinson, J. Crudele, W. D. Johnston, and R. C. Johnson, *J. Biomed. Mater. Res.* **29**, 1517-1524 (1995).
- 83 D. W. Hutmacher, *Biomaterials* **21**, 2529-2543 (2000).
- 84 S. F. Yang, K. F. Leong, Z. H. Du, and C. K. Chua, *Tissue Eng.* **8**, 1-11 (2002).
- 85 M. D. Pierschbacher and E. Ruoslahti, *Nature* **309**, 30-33 (1984).
- 86 S. P. Massia and J. A. Hubbell, *Ann. N.Y. Acad. Sci.* **589**, 261-270 (1990).
- 87 D. A. Barrera, E. Zylstra, P. T. Lansbury, and R. Langer, *J. Am. Chem. Soc.* **115**, 11010-11011 (1993).
- 88 B. D. Ratner, *J. Mol. Recognition* **9**, 617-625 (1996).
- 89 U. Hersel, C. Dahmen, and H. Kessler, *Biomaterials* **24**, 4385-4415 (2003).
- 90 P. G. Robey, *Connect. Tissue Res.* **35**, 131-6 (1996).
- 91 A. L. Boskey, *Connect. Tissue Res.* **35**, 357-63 (1996).

- 92 J. Holland, L. Hersh, M. Bryhan, E. Onyiriuka, and L. Ziegler, *Biomaterials* **17**, 2147-2156 (1996).
- 93 A. D. Cook, J. S. Hrkach, N. N. Gao, I. M. Johnson, U. B. Pajvani, S. M. Cannizzaro, and R. Langer, *J. Biomed. Mater. Res.* **35**, 513-523 (1997).
- 94 J. B. Thompson, J. H. Kindt, B. Drake, H. G. Hansma, D. E. Morse, and P. K. Hansma, *Nature* **414**, 773-776 (2001).
- 95 T. Kokubo, H. Kushitani, S. Sakka, T. Kitsugi, and T. Yamamuro, *J. Biomed. Mater. Res.* **24**, 721-734 (1990).
- 96 T. Kokubo, *Acta Mater.* **46**, 2519-2527 (1998).
- 97 R. Y. Zhang and P. X. Ma, *J. Biomed. Mater. Res.* **45**, 285-293 (1999).
- 98 S.-H. Rhee and J. Tanaka, *Biomaterials* **20**, 2155-2160 (1999).
- 99 R. Y. Zhang and P. X. Ma, *J. Biomed. Mater. Res.* **44**, 446-455 (1999).
- 100 R. Labella, M. Braden, and S. Deb, *Biomaterials* **15**, 1197-1200 (1994).
- 101 A. M. P. Dupraz, J. R. deWijn, S. A. T. vanderMeer, and K. deGroot, *J. Biomed. Mater. Res.* **30**, 231-238 (1996).
- 102 D. N. Misra, *J. Dent. Res.* **12**, 1405-1408 (1985).
- 103 J.-H. Bradt, M. Mertig, A. Teresiak, and W. Pompe, *Chem. Mater.* **11**, 2694-2701 (1999).
- 104 Q. Liu, J. R. de Wijn, D. Bakker, M. van Toledo, and C. A. van Blitterswijk, *J. Mater. Sci. - Mater. Med.* **9**, 23-30 (1998).
- 105 Q. Liu, J. R. de Wijn, and C. A. van Blitterswijk, *J. Biomed. Mater. Res.* **40**, 257-263 (1998).
- 106 Q. Liu, J. R. de Wijn, and C. A. van Blitterswijk, *J. Biomed. Mater. Res.* **40**, 358-364 (1998).

- 107 W. L. Murphy and D. J. Mooney, *J. Am. Chem. Soc.* **124**, 1910-1917 (2002).
- 108 A. J. Phillips and J. Stone, *Contact Lenses* (Butterworth & Co., London, Boston, 1989).
- 109 A. Kidane, J. M. Sxabocsik, and K. Park, *Biomaterials* **19**, 2051-2055 (1998).
- 110 H. R. Oxley, P. H. Corkhill, J. H. Fitton, and B. J. Tighe, *Biomaterials* **14**, 1064-1072
(1993).
- 111 L. Flynn, P. D. Dalton, and M. S. Shoichet, *Biomaterials* **24**, 4265-4272 (2003).
- 112 J. P. W. Vermeiden, B. B. Rejda, J. G. J. Peelen, and K. de Groot, in *Evaluation of
Biomaterials*, edited by G. D. Winter, J. L. Leray, and K. de Groot (Wiley, New York,
1980), p. 405-411.
- 113 J. M. Yang, J. W. You, H. L. Chen, and C. H. Shih, *J. Biomed. Mater. Res.* **33**, 83-88
(1996).
- 114 C. Prati, R. Mongiorgi, G. Valdre, and G. Montanary, *Clin. Mater.* **8** (1991).
- 115 S. Lu and K. S. Anseth, *J. Controlled Release* **57**, 291-300 (1999).
- 116 M. V. Sefton, M. H. May, S. Lahooti, and J. E. Babensee, *J. Controlled Release* **65**, 173-
186 (2000).
- 117 G. H. Nancollas and J. Zhang, in *Hydroxyapatite and Related Materials*, edited by P. W.
Brown and B. Constantnz (CRC, Boca raton, 1994), p. 73.
- 118 H. A. Lowenstam and S. Weiner, *On Biomineralization* (Oxford University Press,
Oxford, 1989).
- 119 G. H. Nancollas, in *Biomineralization. Chemical and Biochemical Perspectives*, edited by
S. Mann, J. Webb, and R. J. P. Williams (VCH Publishers, Weinheim, 1989), p. 157-187.
- 120 L. Addadi, S. Raz, and S. Weiner, *Adv. Mater.* **15**, 959-970 (2003).

- 121 J. Aizenberg, G. Lambert, S. Weiner, and L. Addadi, *J. Am. Chem. Soc.* **124**, 32-39
(2002).
- 122 T. M. Freyman, I. V. Yannas, and L. J. Gibson, *Prog. Mater. Sci.* **46**, 273-282 (2001).
- 123 G. K. Hunter, *Curr. Opin. Solid State Mater. Sci.* **1**, 430-435 (1996).
- 124 J. Garside, in *Biological Mineralization and Demineralization*, edited by G. H. Nancollas
(Springer-Verlag, Berlin, 1982), p. 23-35.
- 125 S. Weiner and L. Addadi, *J. Mater. Chem.* **7**, 689-702 (1997).
- 126 A. Berman, D. J. Ahn, A. Lio, M. Salmeron, A. Reichert, and D. Charych, *Science* **269**,
515-518 (1995).
- 127 G. F. Xu, N. Yao, I. A. Aksay, and J. T. Groves, *J. Am. Chem. Soc.* **120**, 11977-11985
(1998).
- 128 G. F. Xu, I. A. Aksay, and J. T. Groves, *J. Am. Chem. Soc.* **123**, 2196-2203 (2001).
- 129 S. Okada, S. Peng, W. Spevak, and D. Charych, *Acc. Chem. Res.* **31**, 229-239 (1998).
- 130 J. Song, Q. Cheng, S. Kopta, and R. C. Stevens, *J. Am. Chem. Soc.* **123**, 3205-3213
(2001).
- 131 E. M. Landau, M. Levanon, L. Leiserowitz, M. Lahav, and J. Sagiv, *Nature* **318**, 353-358
(1985).
- 132 X. K. Zhao, J. Yang, L. D. McCormick, and J. H. Fendler, *J. Phys. Chem.* **96**, 9933-9939
(1992).
- 133 B. R. Heywood and S. Mann, *Adv. Mater.* **6**, 9-20 (1994).
- 134 S. Rajam, B. R. Heywood, J. B. A. Walker, S. Mann, R. J. Davey, and J. D. Birchall, *J.*
Chem. Soc., Faraday Trans. **87**, 727-734 (1991).
- 135 J. Aizenberg, A. J. Black, and G. M. Whitesides, *Nature* **398**, 495-498 (1999).

- 136 J. Aizenberg, A. J. Black, and G. M. Whitesides, *J. Am. Chem. Soc.* **121**, 4500-4509
(1999).
- 137 J. N. Israelachvili, *Intermolecular and Surface Forces* (Academic Press, London, 1992).
- 138 T. A. Langworthy, *Curr. Top. Membr. Transp.* **17**, 45-77 (1982).
- 139 J. Song, Q. Cheng, and R. C. Stevens, *Chem. Phys. Lipids* **114** (2002).
- 140 J. Song, J. S. Cisar, and C. R. Bertozzi, (submitted).
- 141 S. I. Stupp and G. W. Ciegler, *J. Biomed. Mater. Res.* **26**, 169-183 (1992).
- 142 S. I. Stupp, J. A. Hanson, J. A. Eurell, G. W. Ciegler, and A. Johnson, *J. Biomed. Mater.
Res.* **27**, 301-311 (1993).
- 143 S. I. Stupp, G. C. Mejicano, and J. A. Hanson, *J. Biomed. Mater. Res.* **27**, 289-299
(1993).
- 144 A. Firouzi, D. Kumar, L. M. Bull, T. Besier, P. Sieger, Q. Huo, S. A. Walker, J. A.
Zasadzinski, C. Glinka, J. Nicol, D. I. Margolese, G. D. Stucky, and B. F. Chmelka,
Science **267**, 1138-1143 (1995).
- 145 T. M. G. Chu, J. W. Halloran, S. J. Hollister, and S. E. Feinberg, *J. Mater. Sci. - Mater.
Med.* **12**, 471-478 (2001).
- 146 T. M. G. Chu, S. J. Hollister, J. W. Halloran, S. E. Feinberg, and D. G. Orton, in
Reparative Medicine: Growing Tissues and Organs; Vol. 961 (2002), p. 114-117.
- 147 J. M. Taboas, R. D. Maddox, P. H. Krebsbach, and S. J. Hollister, *Biomaterials* **24**, 181-
194 (2003).
- 148 G. A. Brady and J. W. Halloran, *J. Mater. Sci.* **33**, 4551-4560 (1998).

- ¹⁴⁹ K. J. L. Burg, W. D. Holder, C. R. Culberson, R. J. Beiler, K. G. Greene, A. B. Loeb sack, W. D. Roland, P. Eiselt, D. J. Mooney, and C. R. Halberstadt, *J. Biomed. Mater. Res.* **51**, 642-649 (2000).
- ¹⁵⁰ B. Jeong, Y. H. Bae, D. S. Lee, and S. W. Kim, *Nature* **388**, 860-862 (1997).
- ¹⁵¹ J. Elisseeff, W. McIntosh, K. Anseth, S. Riley, P. Ragan, and R. Langer, *J. Biomed. Mater. Res.* **51**, 164-171 (2000).
- ¹⁵² A. K. Salem, F. R. A. J. Rose, R. O. C. Oreffo, X. B. Yang, M. C. Davies, J. R. Mitchell, C. J. Roberts, S. Stolnik-Trenkic, S. J. B. Tendler, P. M. Williams, and K. M. Shakesheff, *Adv. Mater.* **15**, 210-213 (2003).

Figures Legends:

Figure 1: Preparation of an environmentally responsive gel by selective conjugate addition.

A mono-functional peptide containing an integrin-binding RGDSP ligand for cell adhesion was reacted with a precursor containing multi-armed end-functionalized PEG macromers. A bifunctional peptide was used to crosslink the assembly. The bifunctional peptide determines the response of the material in the presence of cell-secreted enzymes, in this case, MMPs. These building blocks lead to the formation of elastic gel networks, which degrade to soluble products upon exposure to MMPs by cleavage of the crosslinking peptides. Reprinted with permission from Ref. 27, M. P. Lutolf et al., *Nature Biotechnology* **21**, 513-518 (2003). Copyright 2003 Nature.

Figure 2. Mimicking bone biogenesis using a synthetic biomineralization scaffold.

Figure 3. Assembling of a hydrogel scaffold containing multiple functional domains and the monomers displaying various anionic or adhesive side chains. Note that the anionic monomers differ in both the type of anionic residues and the number of anionic charges carried per side chain.

Figure 4. Morphology, crystallinity, and mineral-gel interfacial affinity of calcium phosphate apatite layer grown on the surface of pHEMA. (A) SEM showing 2-dimensional circular outward growth of calcium apatite from multiple nucleation sites on the acidic surface of pHEMA. (B) SEM showing the merge of circular mineral layers and the full coverage of the

hydrogel surface with calcium apatite. (C) SEM showing an indent formed on the surface of mineralized pHEMA using a Vickers microindenter with a load of 5 N. The calcium phosphate layer did not delaminate. (D) SEM-associated EDS area analysis of the mineral layer shown in micrograph B, confirming the chemical composition and Ca/P ratio (1.6 ± 0.1) that is typical for HA. Synthetic HA was used to calibrate the determination of the Ca/P ratio. (E) X-ray diffraction patterns of the pHEMA composite (a) and unmineralized pHEMA gel (b). The lack of diffraction peaks corresponding to crystalline HA suggests that an amorphous or nanocrystalline layer was formed on the pHEMA surface. In all cases, mineralization was carried out for 2 hrs. Reprinted with permission from Ref. 51, J. Song et al., *J. Am. Chem. Soc.* **125**, 1236-1243 (2003). Copyright 2003 American Chemical Society.

Figure 5. A urea-mediated mineral growth patterns on pHEMA based copolymers displaying various anionic residues. Materials studied were pHEMA with 5% Glu-MA (A), 5% Gly-MA (B) and 5% Ser-MA (C). Note that the deliberate fracturing of the composite (B) did not lead to delamination of any circular mineral domains, suggesting an excellent gel-mineral interfacial adhesion strength.

Figure 6. A cartoon illustration of oriented calcite growth on the surface of a polydiacetylene (PDA) thin film driven by cooperative interactions at the polymer-mineral interface. The self-assembling lipid was first spread and compressed on the surface of a standard trough. UV irradiation of the compressed film resulted in topochemically polymerized blue PDA film, which was then horizontally transferred to hydrophobized solid support (not drawn here). Template-driven mineralization of calcite was initiated by supersaturated CaCO_3 solution placed

on the PDA film. The cooperative interactions led to structural reorientation of the polymer template, accompanied by a blue-to-red chromatic transition of the PDA film, and co-alignment of calcite at the anionic surface, with the (012) plane oriented parallel to the PDA membrane plane.

Figure 7. Rational design of a functional self-assembling peptide amphiphile. (A) Chemical structure of the peptide amphiphile, highlighting five key structural features. Region 1 is a long alkyl tail that conveys hydrophobic character to the molecule and, when combined with the peptide region, makes the molecule amphiphilic. Region 2 is composed of four consecutive cysteine residues that when oxidized may form disulfide bonds to polymerize the self-assembled structure. Region 3 is a flexible linker region of three glycine residues to provide the hydrophilic head group flexibility from the more rigid cross-linked region. Region 4 is a single phosphorylated serine residue that is designed to interact strongly with calcium ions and help direct mineralization of hydroxyapatite. Region 5 displays the cell adhesion ligand RGD. (B) Molecular model of the PA showing the overall conical shape of the molecule going from the narrow hydrophobic tail to the bulkier peptide region. Color scheme: C, black; H, white; O, red; N, blue; P, cyan; S, yellow. (C) Schematic showing the self-assembly of PA molecules into a cylindrical micelle. Reprinted with permission from Ref. 26, J. D. Hartgerink et al., *Science* **294**, 1684-1688 (2001) Copyright 2001 American Association for the Advancement of Science.

Figure 8. A library of bolaamphiphilic diacetylene lipids displaying a wide range of surface residues. Diacetylene group, the potential polymerization site, is designed to locate at the center of the lipophilic core of each bolaamphiphile. The R- group carried on one end of each lipid is

either neutral (**1**), anionic (**2-8**) or zwitterionic (**9**). The anionic groups differ in both the type of anionic residues and the number of negative charges they carry. All bolaamphiphiles (**1-9**) are synthesized from a common precursor, NHS-activated lipid **10**.

Figure 9. Transmission electron micrographs, contact mode atomic force microscopy images and the corresponding unit cell dimensions of Poly-L-Glu-Bis-3 adopting flat (panel A) and twisted (panel B) ribbon morphologies. Adapted with permission from Ref. 130, J. Song et al., *J. Am. Chem. Soc.* **123**, 3205-3213 (2001). Copyright 2003 American Chemical Society.

Figure 10. A polyelectrolyte strategy towards 3-dimensional BPDA-calcium apatite composites.

Scheme 1. Urea-Mediated Solution Mineralization of Hydroxyapatite (HA) onto pHEMA Hydrogel Scaffolds. Thermo-decomposition of urea produces a gradual increase in pH, resulting in the hydrolysis of surface 2-hydroxyethyl esters (A) and the precipitation of HA from the aqueous solution. The in situ generated surface carboxylates strongly interact with calcium ions (B) and facilitate the heterogeneous nucleation and 2-dimensional growth of a high-affinity calcium-phosphate (CP) layer on the pHEMA surface (C). Prolonged mineralization allows for the growth of a thicker CP layer that covers the entire hydrogel surface as shown in D. A proposed urea-mediated, pH-dependent HA nucleation and growth behavior from the solution in qualitatively depicted by the red dotted curve shown in E (curve 1, the solubility of HA, was taken from reference 117), guiding the chemical and physical transformation of the pHEMA

hydrogel to a highly integrated Gel-CP composite. Reprinted with permission from Ref. 51, J. Song et al., *J. Am. Chem. Soc.* **125**, 1236-1243 (2003). Copyright 2003 American Chemical Society.

Figures:

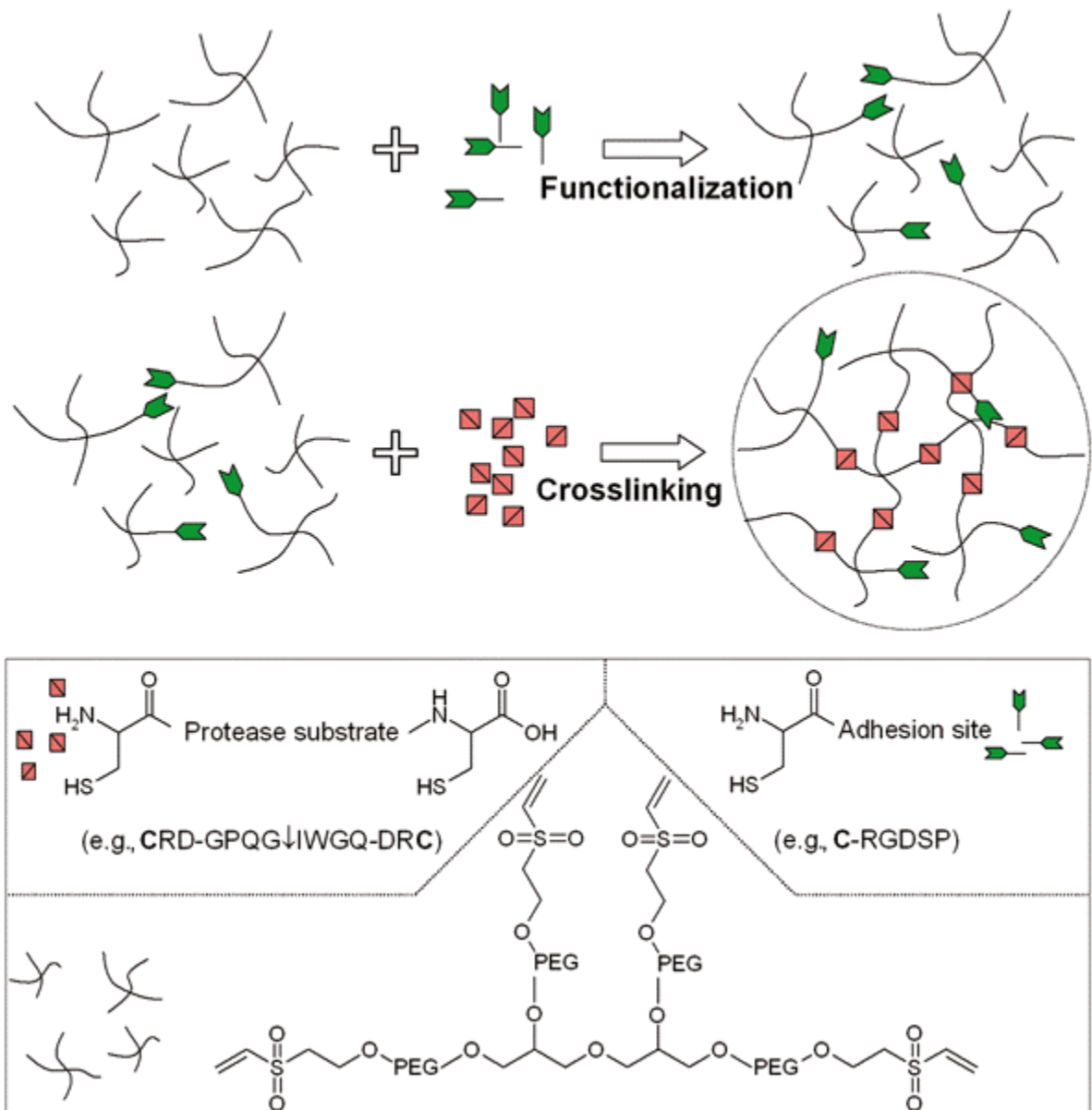


Figure 1

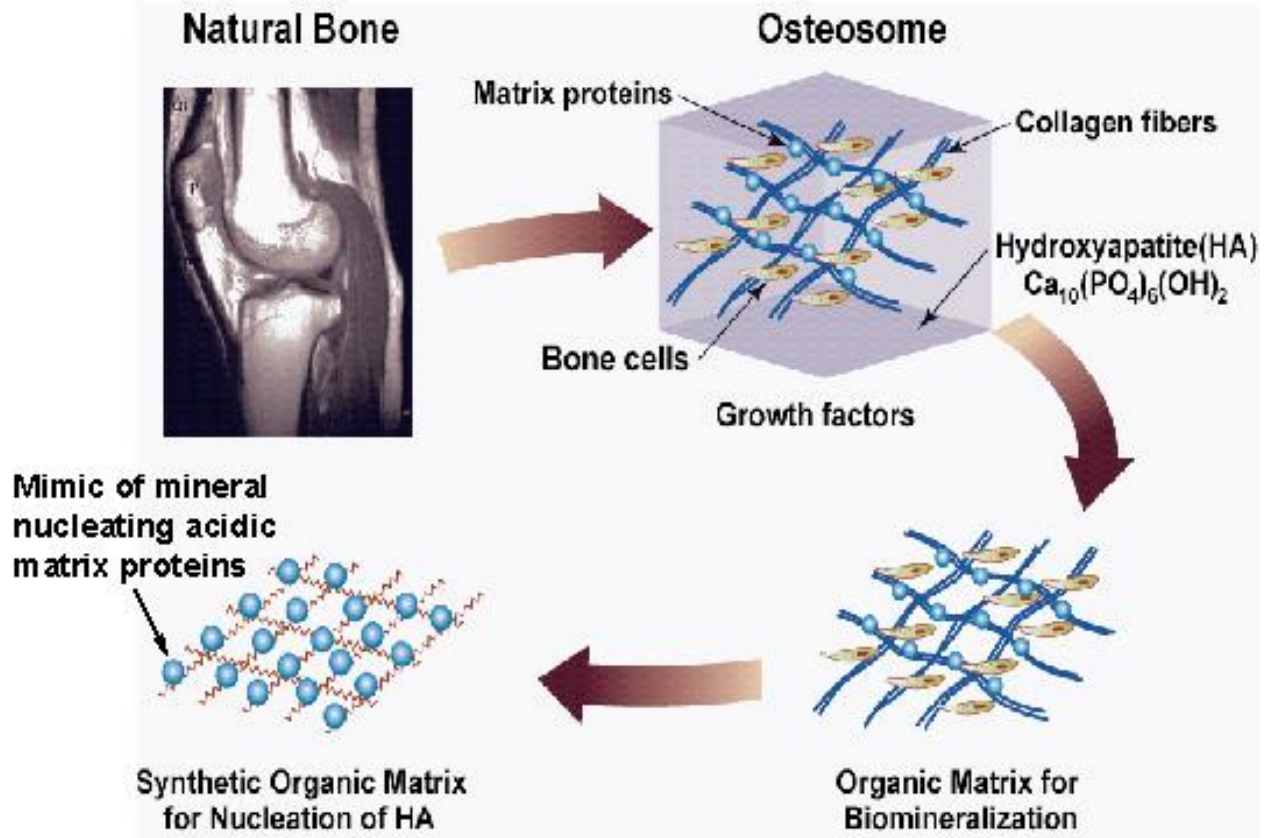


Figure 2

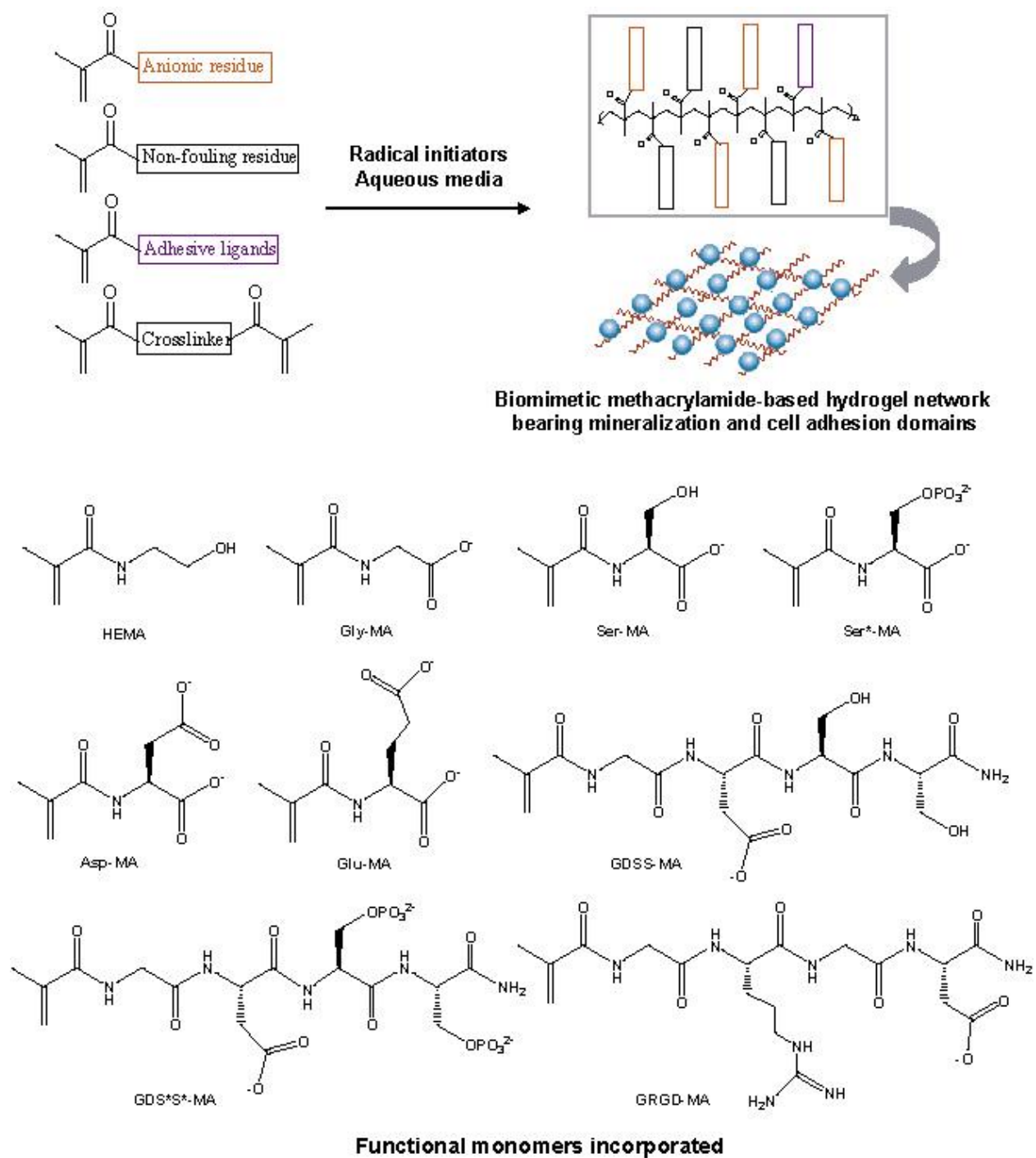


Figure 3

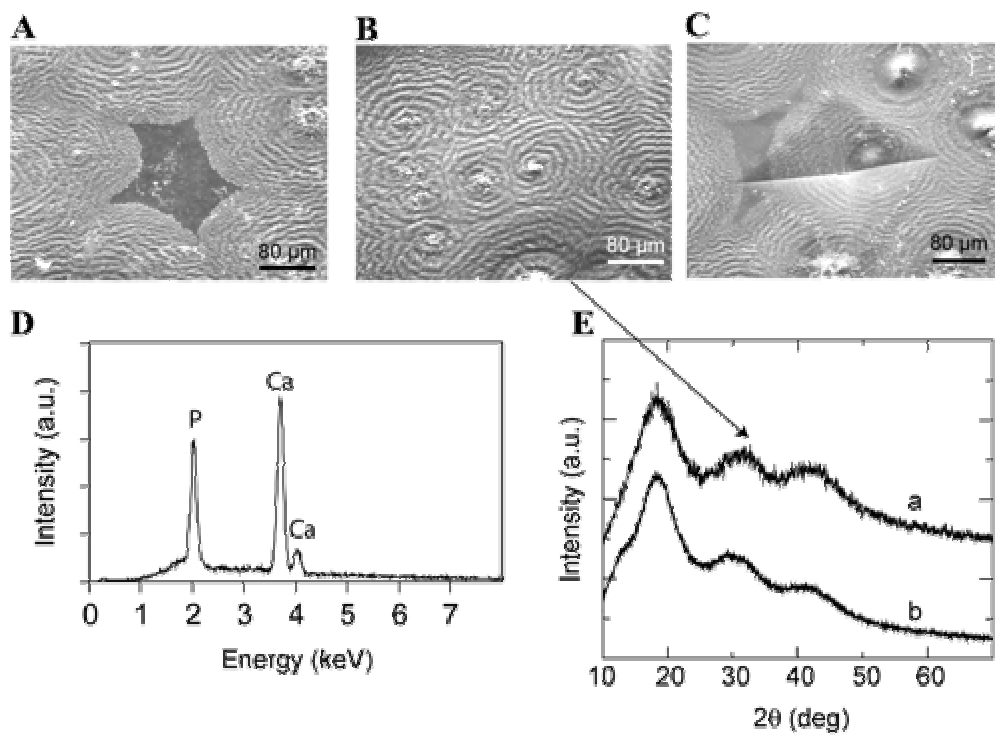


Figure 4

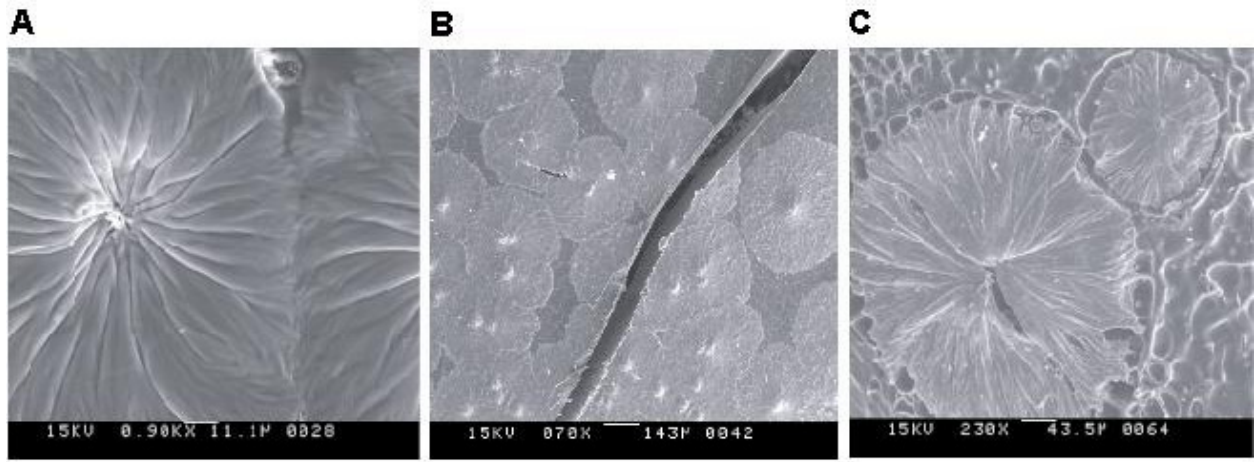


Figure 5

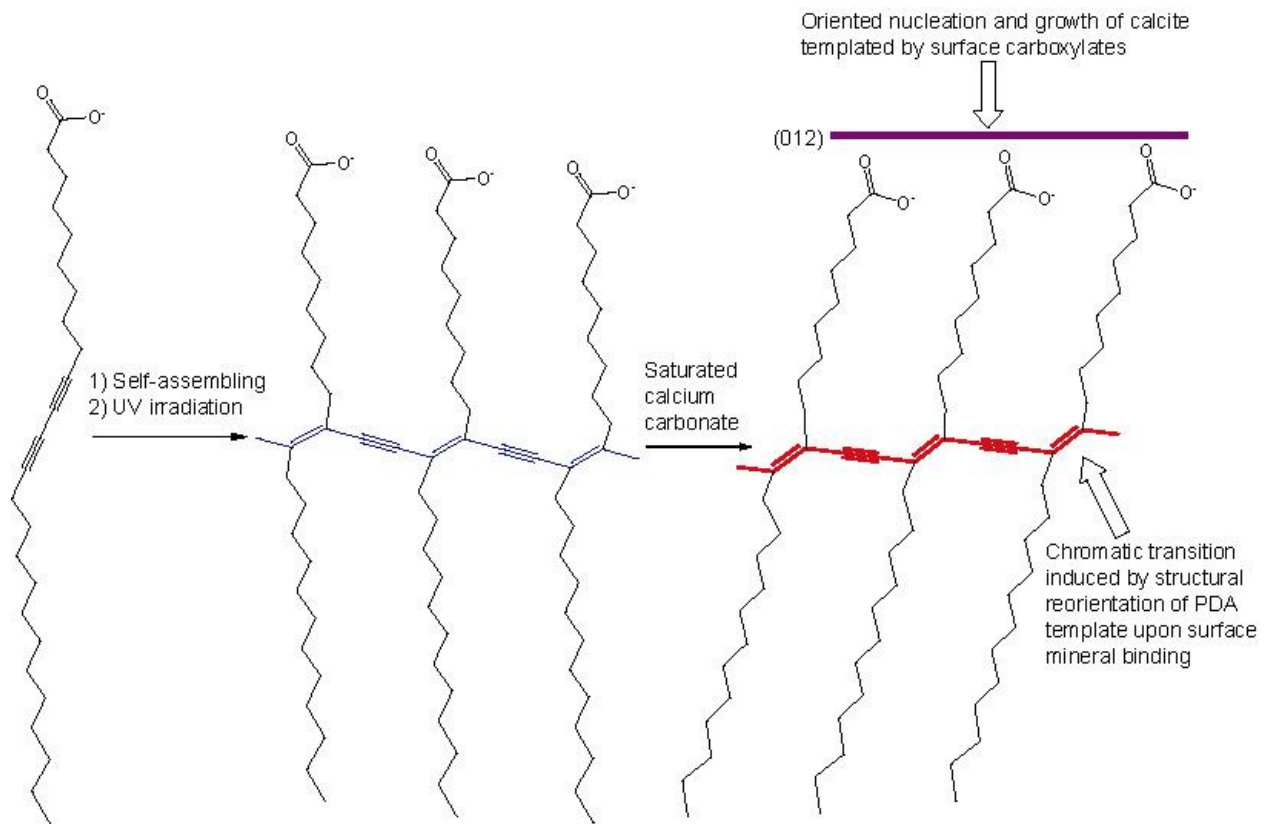


Figure 6

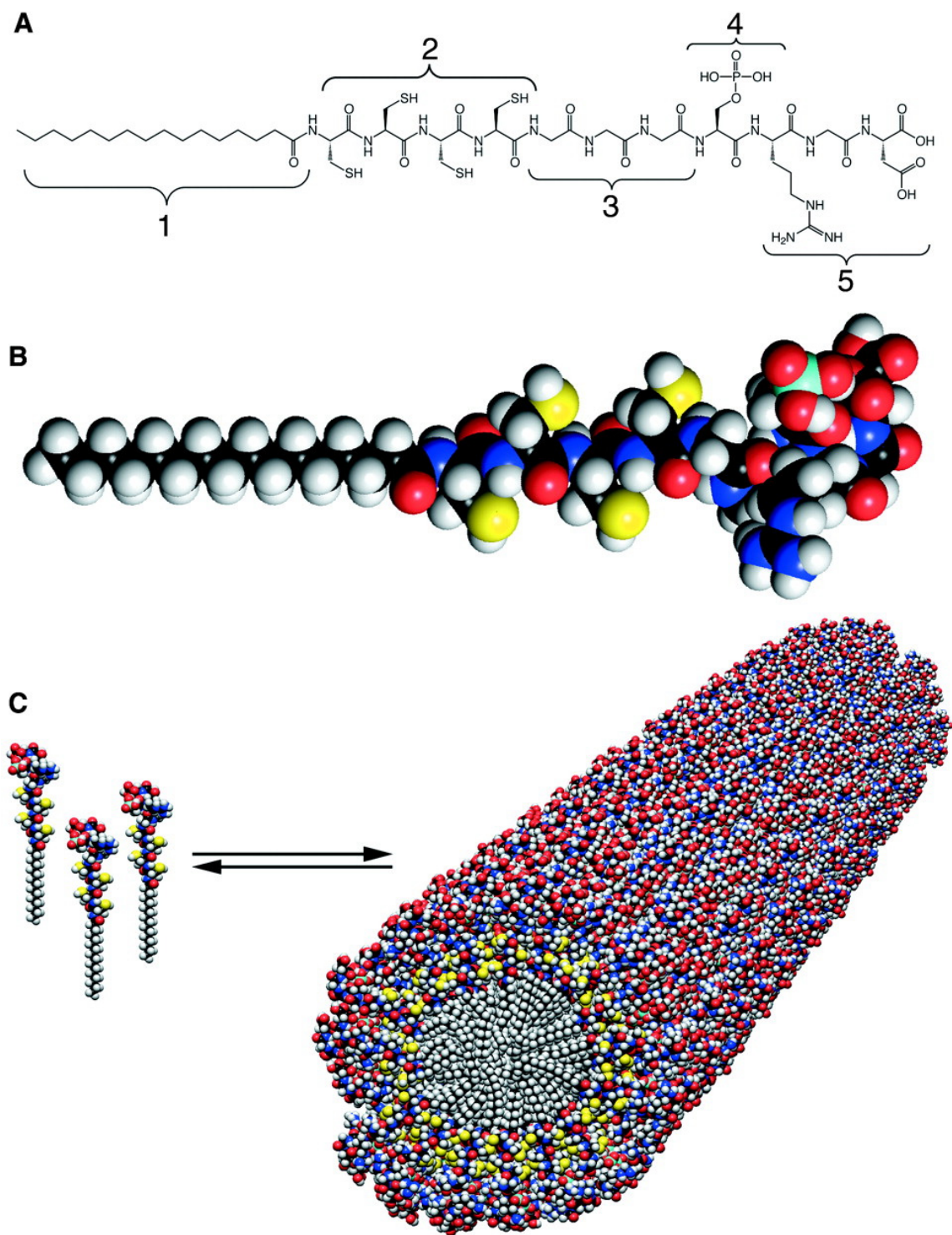


Figure 7

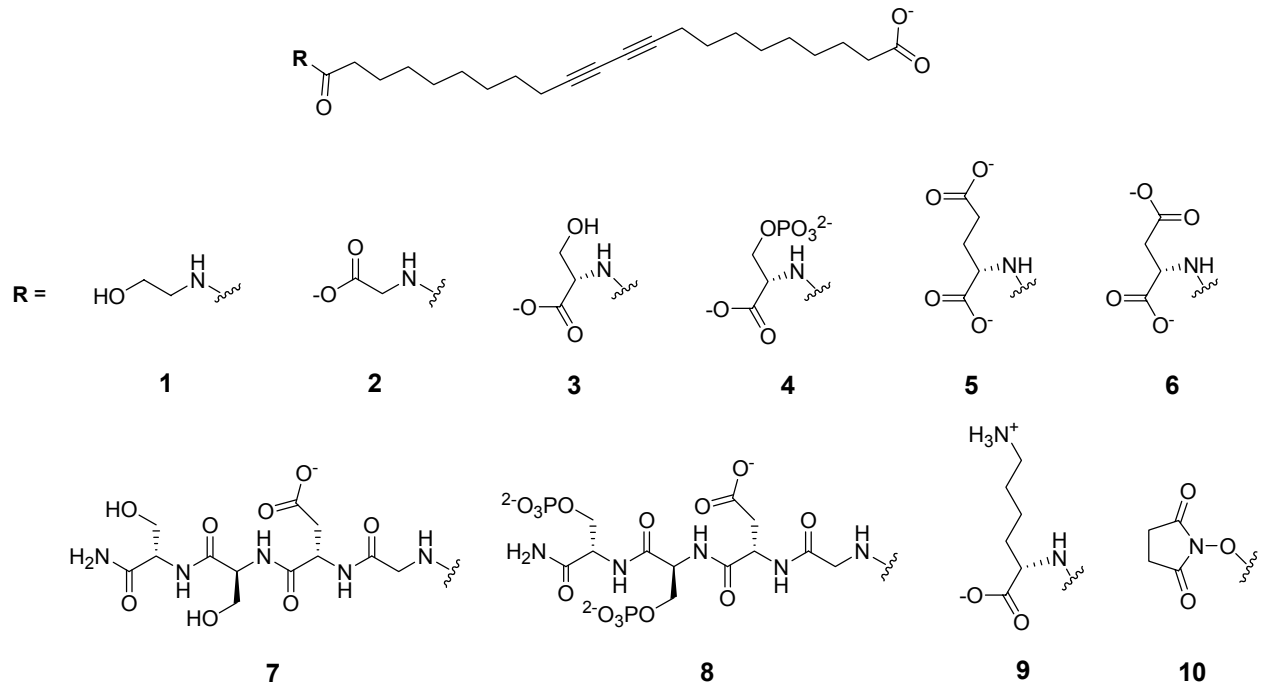
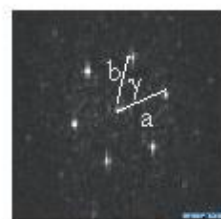
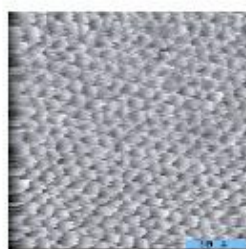
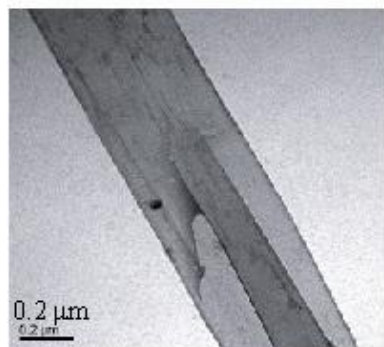


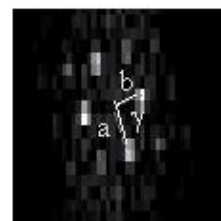
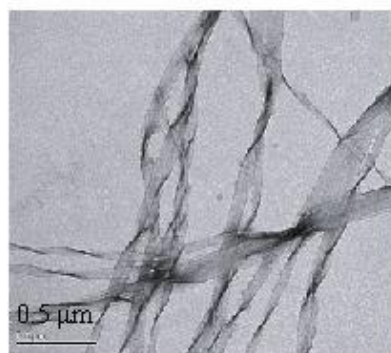
Figure 8

A



$$a = b = 4.8 \pm 0.2 \text{ \AA}; \gamma = 60 \pm 3^\circ$$

B



$$a = 6.1 \pm 0.3 \text{ \AA}; b = 3.9 \pm 0.3 \text{ \AA} \\ \gamma = 92 \pm 3^\circ$$

Figure 9

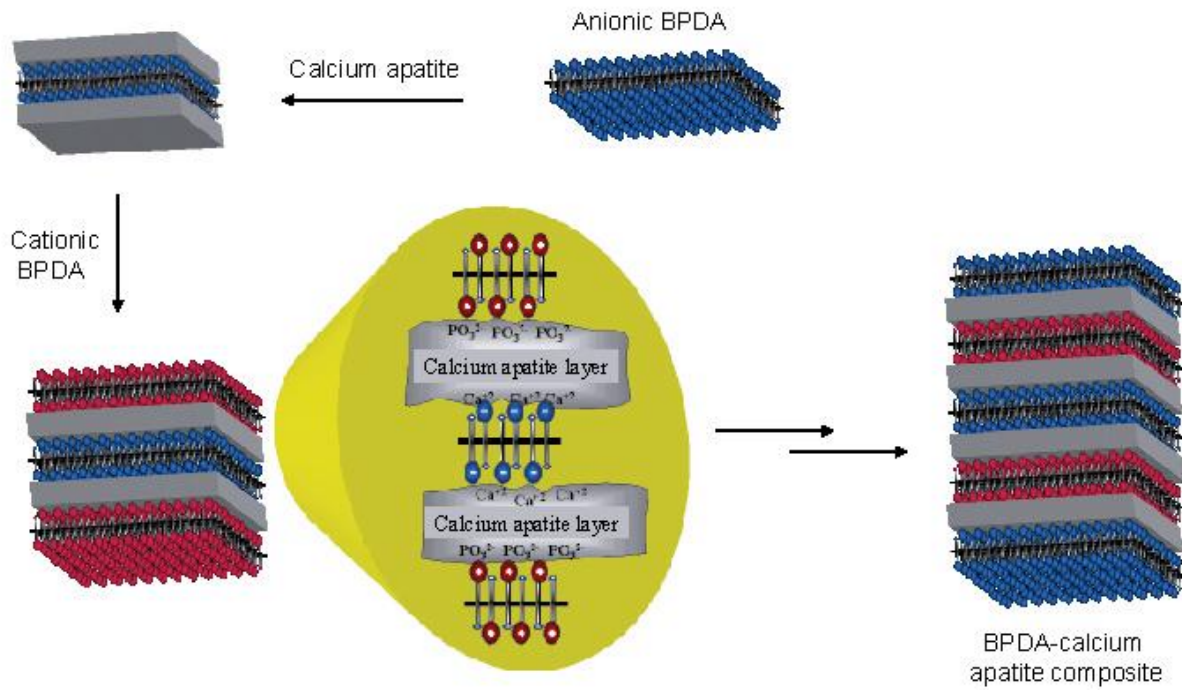
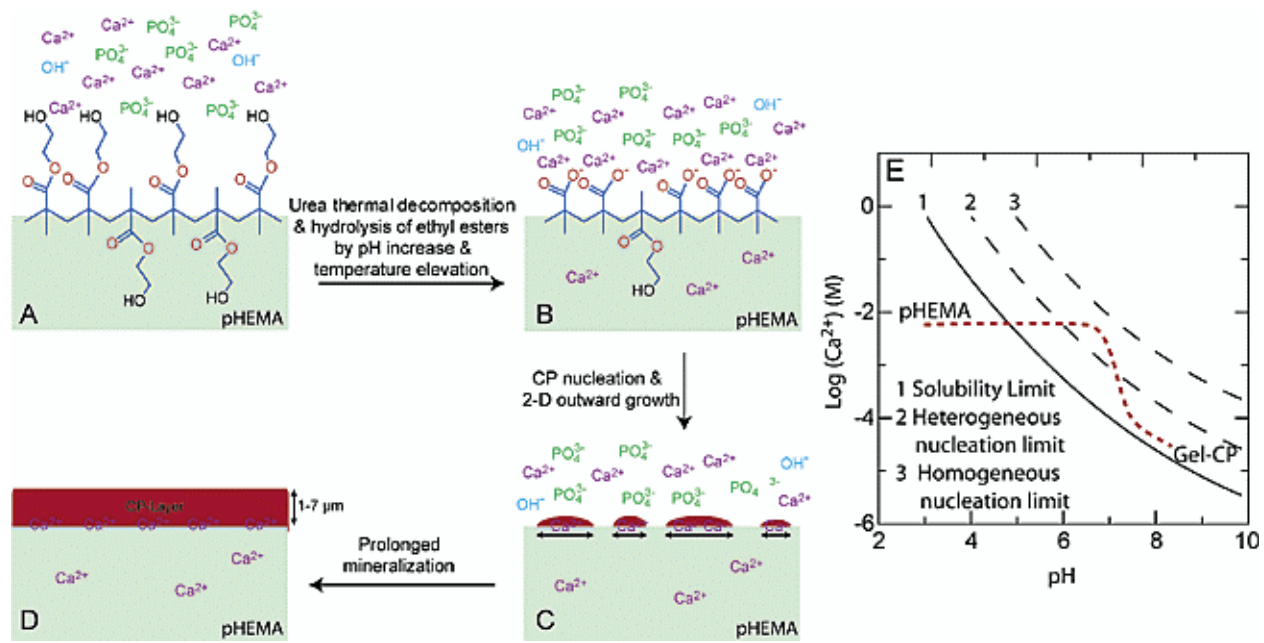


Figure 10



Scheme 1